Research papers

Chance-constrained model predictive control-based operation management of more-electric aircraft using energy storage systems under uncertainty

Xin Wang [a,*], Najmeh Bazmohammadi [b], Jason Atkin [c], Serhiy Bozhko [a], Josep M. Guerrero [b]

[a] Department of Electrical and Electronic Engineering, Faculty of Engineering, University of Nottingham, Nottingham NG7 2RD, UK
[b] Centre for Research on Microgrids (CROM), AAU Energy, Aalborg University, Aalborg 9220, Denmark
[c] Computational Optimisation and Learning Lab, School of Computer Science, University of Nottingham, Nottingham NG7 2RD, UK

ABSTRACT

On more electric aircraft (MEA), reducing fuel consumption and guaranteeing flight safety are pursued by efficient operational management of the electrical power system (EPS). Considering the growing number of onboard electric loads and the increasing complexity of EPS architecture due to the integration of multiple power converters and energy storage systems (ESSs), system-level operation control is required to manage power distribution, load scheduling, and ESSs. In this paper, a chance-constrained stochastic model predictive control (CC-SMPC) method is proposed to improve both the system operation in terms of the system's cost and reconfiguration activities as well as the ability to cope with uncertainties due to fluctuating load demands. Both normal and faulty operating conditions are investigated with multi-failure cases, resulting in different uncertainty propagation paths. The system's operational and technical requirements are formulated as a set of deterministic and probabilistic constraints in the CC-SMPC model. To verify the effectiveness of the proposed strategy, a comprehensive comparison study is conducted. Two uncertainty/failure cases are taken into account and simulations are performed for both offline and online control strategies while the Monte-Carlo algorithm is used for scenario generation. The results are evaluated using the proposed evaluation framework, showing that the CC-SMPC achieves better performance compared to deterministic MPC (DMPC) in both cases. In an offline testing framework, comparing the performance of DMPC and CC-SMPC strategies shows that CC-SMPC reduces the power constraint violations for batteries and generators in all cases following the selected confidence level. In addition, in an online testing framework with 1 % violation probability, the following results are observed in the two cases: In the EPS normal condition, CC-SMPC reduces the total cost by 31.4 % and the overall constraint violation cost by 93 %; while in the EPS faulty condition, CC-SMPC reduces the total cost by 4.37 %, and the overall constraint violation cost by 96 %.

Nomenclature

Indices of EPS architecture		
j, l		Index for HV and LV buses respectively
c		Index for DC/DC converter
p, q		Index for HV and LV loads respectively
N^{APU}		Number of APU
N^{HVB}		Number of HV buses
N^{LVB}		Number of LV buses
N^C		Number of DC/DC converters
N^{BAT}		Number of batteries
Parameters of EPS		
Power limitations	P_j^{Gmax}	Maximum output power of generator j [kW]

(continued on next column)

(continued)

	P^{APUmax}	Maximum output power of APU [kW]
	$P_{jj'}^{HVmax}$	Maximum power of HV buses [kW]
	P_{jc}^{HVCmax}	Maximum power of connection link between HV bus j and DC/DC converter c [kW]
	P_{cl}^{LVCmax}	Maximum power of connection link between DC/DC converter c and LV bus j [kW]
	P_l^{BATmax}	Maximum power for each battery l [kW]
	$P_{l'}^{LVmax}$	Maximum power of LV buses [kW]
ESS limitations	B_l^{cap}	Capacity of battery l [kWh]

(continued on next page)

(*continued*)

	HI, LO	Upper/Lower boundary for battery state of charge
Efficiency	η_{lj}^{AHV}	Transmission efficiency in cables between the APU bus and HV bus j
	$\eta_{ljj'}^{HV}$	Transmission efficiency in cables of HV bus connection between bus j and j'
	η_{ljc}^{HVC}	Transmission efficiency in cables between the HV bus j and DC/DC converter c
	η_c	Efficiency of DC/DC converter c
	η_{cl}^{LVC}	Transmission efficiency in cables between the DC/DC converter c and LV bus l
	η_l^{BAT}	Charging/ Discharging efficiency of battery l
	$\eta_{ll'}^{LV}$	Transmission efficiency in cables of LV bus connection between bus l and l'
Load priority	$\lambda_{jp}^{HVLncri}$	The priority of the pth non-critical load on HV bus j
	$\lambda_{jq}^{LVLncri}$	The priority of the qth non-critical load on LV bus l
Parameters of DMPC/CC-SMPC		
Load power	$P_{jp}^{HVLcri}(k)$	The pth critical load power on HV bus j [kW]
	$P_{jp}^{HVLncri}(k)$	The pth non-critical load power on HV bus j [kW]
	$P_{lq}^{LVLcri}(k)$	The qth critical load power on LV bus l [kW]
	$P_{lq}^{LVLncri}(k)$	The qth non-critical load power on LV bus l [kW]
Failure	$\gamma_j^G(k)$	Indicator for the failure of generator j
	$\gamma_{jc}^{HVC}(k)$	Indicator for the failure of connection link between HV bus j and DC/DC converter c
	$\gamma_{cl}^{LVC}(k)$	Indicator for the failure of connection link between DC/DC converter c and LV bus l
	$\gamma^C(k)$	Indicator for the failure of DC/DC converter c
	$\gamma_l^{BAT}(k)$	Indicator for the failure of battery l
Continuous decision variables of DMPC/CC-SMPC		
Power	$P^{APU}(k)$	Power flowing from APU to the APU bus [kW]
	$P_j^{AHVp}(k)$	Power flowing from APU bus to the HV bus j [kW]
	$P_j^{AHVn}(k)$	Power flowing from HV bus j to the APU bus [kW]
	$P_j^G(k)$	Power flowing from generator j to corresponding HV bus j [kW]
	$P_{jj'}^{HV}(k)$	Power flowing from HV bus j to HV bus j' [kW]
	$P_{jc}^{HVC}(k)$	Power flowing from HV bus j to DC/DC converter c [kW]
	$P_{cl}^{LVC}(k)$	Power flowing from DC/DC converter c to LV bus l [kW]
	$P_l^{BAT}(k)$	Power of battery on LV bus l [kW]
	$P_{ll'}^{LV}(k)$	Power flowing from LV bus l to LV bus l' [kW]
ESS	$SOC_l(k)$	State of charge of battery on LV bus l
	$\vartheta_l(k)$	Tolerance for upper bound of state of charge of battery on LV bus l
	$\varepsilon_l(k)$	Tolerance for lower bound of state of charge of battery on LV bus l
Binary decision variables of DMPC/CC-SMPC		
Connections	$S^{APU}(k)$	Connection status of the link between APU and APU bus
	$S_j^{AHV}(k)$	Connection status of the link between APU bus and HV bus j
	$S_j^G(k)$	Connection status of the link between generator j and corresponding HV bus j
	$S_{jj'}^{HV}(k)$	Connection status of the link between HV bus j and HV bus j'
	$S_{jp}^{HVLncri}(k)$	Connection status of the pth non-critical load power on HV bus j
	$S_{jc}^{HVC}(k)$	Connection status of the link between HV bus j and DC/DC converter c
	$S_{cl}^{LVC}(k),$	Connection status of the link between DC/DC converter c and LV bus l
	$S_l^{BAT}(k)$	Connection status of the link between LV bus l and its corresponding battery

(*continued on next column*)

(*continued*)

	$S_{ll'}^{LV}(k)$	Connection status of the link between LV bus l and LV bus l'
	$S_{lq}^{LVLncri}(k)$	Connection status of the qth non-critical load power on LV bus l
	$S^{Phy}(k)$	Vector of physical connections allowing bidirectional power, including $S_j^{AHV}(k)$, $S_{jj'}^{HV}(k)$, $S_l^{BAT}(k)$ and $S_{ll'}^{LV}(k)$
	$S^h(k)$	Vector of physical connections related with failure isolations, including $S_j^G(k)$, $S_l^{BAT}(k)$, $S_{jc}^{HVC}(k)$, and $S_{cl}^{LVC}(k)$.
Indicator of Power direction	$s_j^{AHVp}(k)$	Indicator for power flow direction from APU bus to the HV bus j
	$s_j^{AHVn}(k)$	Indicator for power flow direction from HV bus j to the APU bus
	$s_{jj'}^{HV}(k)$	Indicator for power flow direction HV bus j to HV bus j'
	$s_{j'j}^{HV}(k)$	Indicator for power flow direction HV bus j' to HV bus j
	$s_{ll'}^{LV}(k)$	Indicator for power flow direction from LV bus l to LV bus l'
	$s_{l'l}^{LV}(k)$	Indicator for power flow direction from LV bus l' to LV bus l
	$s_{ll'}^{LV}(k)$	Indicator for power flow direction from LV bus l to LV bus l'
DMPC/CC-SMPC controller parameters		
	H	Prediction horizon [min]
	k	Time intervals, $k \in \mathbb{Z}_{\geq 0}$
	T_s	Sampling time [min]
	N	Total time steps

1. Introduction

1.1. Background and motivation

Among transportation systems, the fastest developments have been observed in the aircraft industry, going from nothing to providing fast, safe, and the most far-reaching travel in only a little more than a century [1]. Environmental issues have been the main focus in the development of all transportation systems in recent years, and this speed of growth in air transportation came with its own environmental problems, since the aviation industry is currently responsible for approximately 2.5 % of global human-induced CO_2 emissions. Therefore, aircraft require more environmentally friendly power systems to meet current CO_2 emission targets. For example, Airbus targets a 50 % reduction in net aviation carbon emissions from 2005 levels by 2050 [2]. To meet these requirements, the concept of more electric aircraft (MEA) has been put forward as the main development tendency for future aircraft, to make air travel more efficient and environmentally friendly.

MEA replace the traditional hydraulics and pneumatics systems with electrical systems to achieve better dynamic responses and higher efficiency, to reduce fuel consumption [3,4]. However, this brings new challenges to the design, control, and operational management of the onboard electrical power system (EPS). Recently, the concepts of flexible power transmission and intelligent application of energy storage (ES) are being explored for onboard EPS. Inspired by this, complex architectures are studied, which integrate generators, high-voltage (HV) and low-voltage (LV) buses, modular power electronic converters, and switches, as well as multiple energy storage systems (ESSs) and different types of loads with higher electrical power demands [5,6]. To cope with the increasingly complex onboard EPS, this paper proposes an optimization-based control strategy for onboard operational management of the MEA, including power distribution scheduling, load management, and energy storage (ES) control. The proposed control system is designed to achieve several control targets while satisfying several technical and operational constraints. In addition, in the EPS of the MEA there exist several safety issues that impose further critical operating requirements, such as faulty components/connections and uncertainties of load demands during the flight. The controller should be able to cope

with different failure scenarios, continuing to supply the safety-related loads. Furthermore, the EPS operational management is also subject to other sources of uncertainties that also need to be appropriately handled. Therefore, a system-level controller is required to meet these critical requirements and guarantee flight safety, while achieving optimized EPS performance under various fault and uncertainty scenarios.

1.2. Literature review

Various controller designs have been proposed in the literature for system-level operational management of the EPS in the MEA, more electric vehicles (MEV), and terrestrial power grids. Although the operational requirements of an MEA are different from those of an MEV and a terrestrial grid, the latter two inspire the research for MEA applications. Rule-based methods in [7–10], and instantaneous optimization methods in [11–14] provide operational solutions based on only the past and current information of the system and cannot account for future system changes, to avoid adverse operating conditions in advance [15]. To avoid worst-case costly operating scenarios, model predictive control (MPC) has been drawing the attention of the power system community for optimal control and operational management of electrical systems [16]. Since MPC accounts for the system's future trajectory when deriving the optimal operating strategy, the worst-case situations can be avoided by taking corrective actions in advance. This benefits aircraft applications that must comply with strict safety requirements. In [17], MPC is used for optimal load management in an aircraft power distribution system while considering generator faults. A hierarchical MPC framework for hybrid propulsion systems is proposed in [18] to decouple the slow and fast response dynamic energy management problems. The MPC method is also applicable for decentralized control. In [19], a distributed MPC is proposed for controlling the engine and the connected electrical power distribution system of an MEA power system.

The abovementioned conventional MPC methods are deterministic, not taking the uncertainty explicitly into account, and are known as deterministic MPC (DMPC). Although the inherent feedback mechanism of DMPC, stemming from its receding horizon mechanism, makes the system more robust compared to other control methods [20,21], the uncertainty of the system can still cause the DMPC to be less effective in providing reliable control strategies than systems which explicitly account for uncertainty. For example, in [17], when DMPC is applied for optimal load management of an aircraft power distribution system, the uncertainty in load demand leads to poor performance due to the imprecise load predictions. Therefore, the authors in [22] propose a chance-constrained stochastic MPC (CC-SMPC) to solve the same onboard load management problem, considering either load demand uncertainty or contactor failures, but not taking both into account simultaneously. In addition, a simple conventional EPS architecture is considered, where the propagation of uncertainty is simplified, with independent loads and buses. Regarding terrestrial power grid applications, in [23–27], CC-SMPC is proposed for the coordinated energy management of microgrids. Although the multi-uncertainty scenario is discussed in these papers, a common grid is applied to compensate for all of the uncertainty, avoiding the interactions of flexible configurations, power scheduling, and uncertainty propagation. In the most recent studies, chance-constrained methods are proposed for unit commitment in [28,29], optimal scheduling of combined cooling, heating, and power-based microgrid in [30], and optimal energy-reserve scheduling of a wind-photovoltaic-hydrogen energy system in [31]. However, there remains a research gap for the management of onboard EPS architectures for MEA in more recent studies, such as the MEA EPS in [8]. Compared to the studies in [28–31] for terrestrial grids, novel onboard EPSs require further research on EPS operation strategies, simultaneously considering technical and safety requirements, the potential for multiple failures, and the propagation of the effects of uncertainty.

Rather than directly formulating uncertainty with chance constraints, some studies solve the optimization problem for several

Table 1
Comparison of this study with recent researches[a].

Reference	Application(1)	Control target(2)					Model type(3)	Failure and uncertainty case study						Results evaluation		Performances	
		SS	TS	PF	ESS	LM		Failure		Uncertainty		Uncertainty propagation(4)	Combined failure and uncertainty	Number of uncertainty scenarios		Operating	CV(5)
								Single	Multi	Single	Multi			Online	Offline		
[17]	MEA	✓	✓	✓	✓	✓	D	✓	✗	✗	✗	✗	✗	Single	✗	✓	✗
[18]	MEA	✗	✗	✓	✓	✓	D	✗	✗	✗	✗	✗	✗	Single	✗	✓	✗
[19]	MEA	✗	✗	✓	✗	✗	D	✗	✗	✗	✗	✗	✗	Single	✗	✓	✗
[22]	MEA	✓	✓	✓	✓	✓	CC	✗	✓	✗	✓	✗	✗	Single	✗	✓	✗
[25]	RG	✗	✗	✓	✗	✗	CC	✗	✗	✗	✓	✗	✗	Single	Multiple	✓	✗
[27]	RG	✗	✗	✓	✗	✗	CC	✗	✗	✗	✓	✓	✗	✗	Multiple	✓	✓
[28]	RG	✓	✗	✓	✓	✓	CC	✗	✗	✗	✓	✗	✗	✗	Multiple	✓	✓
[29]	RG	✗	✓	✓	✓	✓	CC	✗	✗	✗	✓	✗	✗	Single	A few	✓	✓
[30]	RG	✗	✗	✓	✗	✗	CC	✗	✗	✗	✓	✗	✗	✗	A few	✓	✗
[31]	RG	✗	✗	✓	✓	✓	CC	✗	✗	✗	✓	✓	✗	Single	✗	✓	✗
[34]	RG	✗	✗	✓	✓	✗	SB	✗	✗	✓	✗	✗	✗	Single	✗	✓	✗
[36]	RG	✓	✓	✓	✓	✗	SB	✗	✗	✗	✓	✗	✗	✗	A few	✓	✗
[37]	RG	✓	✗	✓	✓	✓	SB	✗	✗	✗	✓	✗	✗	✗	A few	✓	✗
[38]	RG	✓	✓	✓	✓	✓	SB	✗	✗	✗	✓	✗	✗	✗	A few	✓	✗
[39]	RG	✓	✗	✓	✓	✓	SB	✗	✗	✗	✓	✓	✗	✗	A few	✓	✗
[40]	RG	✗	✓	✓	✓	✓	SB	✗	✗	✗	✓	✗	✗	Single	✗	✓	✗
[41]	MEA	✗	✗	✓	✗	✗	SB	✗	✓	✗	✓	✗	✓	Single	✗	✓	✗
This paper	MEA	✓	✓	✓	✓	✗	CC	✓	✓	✗	✓	✓	✓	Multiple	Multiple	✓	✓

[a] (1) In application, RG indicates residential grid. (2) In control target, SS indicates power supply switching; TS indicates transmission switching; PF indicates power flow; ESS indicates energy storage systems; LM indicates load management. (3) In model types, D indicates deterministic model; CC indicates chance constrained model; SB indicates scenario based model. (4) Uncertainty propagation indicates that the uncertainty sources are allocated in a multi-bus EPS, which allows different EPS configurations and corresponding uncertainty propagations. (5) CV indicates analysis and evaluations of constraints violation.

predefined uncertain scenarios at each time step, with each scenario integrating a DMPC model, which is named scenario-based (SB) SMPC. This method is applied for operational scheduling and hourly reconfiguration of the distribution systems in [32], the unit commitment and economic dispatch of power systems while considering the uncertainty of load and renewable energy sources in [33], and energy management of the ESS and distributed energy sources in [34–36]. In the most recent studies, scenario-based models are adopted for the scheduling and pricing strategies of smart grids. For example, SB models are proposed for the unit commitment of energy hubs in [37,38], for the scheduling of smart homes in [39], and for the scheduling of retailers with optimal prices in [40]. In these studies, the uncertainties of demands and different types of energy sources are also considered. In particular, the uncertainty of the market price is considered in [39] and [40]. In addition, in [41], a SB-SMPC strategy is proposed for coordinated engine and power management of the MEA. SB-SMPC methods heavily rely on the selection of predefined uncertain scenarios at each time step. More scenarios normally indicate a better representation of uncertainty; however, this can result in a dramatic increase in the computational time for large-scale systems or systems that contain a large number of decision variables - when fewer scenarios are generated, the desired performance cannot be guaranteed.

1.3. Research gap

By reviewing the above research, it can be found that, compared to the SB-SMPC, CC-SMPC is usually better for accurately formulizing uncertainties and saving computational time. However, there is still a large research gap in the literature regarding the operational control of an EPS (especially for MEA applications) considering multi-failure and multi-uncertainty scenarios with CC-SMPC in both methodology and evaluation aspects. Particularly, Table 1 systematically compares the literature related to MEA EPS and studies of other EPS within three years. From the literature review and Table 1, the research gap is concluded in detail below. To fill this gap, a CC-SMPC strategy for the EPS of an MEA is proposed in this paper to address the following issues.

Firstly, combining both normal and multi-failure scenarios simultaneously with multi-uncertainty issues under chance constraints has not been studied, despite this being increasingly important, but complex, as the MEA EPS develops. On the one hand, there are few studies focused on MEA EPSs, and the EPSs studied are conventional. However, future MEA EPSs tend to allow more flexible configurations and utilize the ESS for power scheduling, with modular converters and buses. This introduces various novel operational constraints, requiring appropriate formulizations to cope with both normal and failure scenarios, which have not been studied before. In addition, flexible configurations, power scheduling, and uncertainty propagation interact with each other, requiring these interactions to be modeled and analyzed to provide reliable decisions for the MEA EPS, which has been lacking in the previous studies.

Further, the performance of the CC-SMPC design should be properly evaluated, to demonstrate the online cost with testing scenarios which follow uncertainty distributions. This is required to verify the effectiveness of the proposed strategy for real-world applications. In the reviewed studies, online testing was conducted with only one uncertainty profile, however, this method lacks the verification of the impacts of the uncertainty distribution when the uncertainty profile changes. These impacts are not considered in the existing evaluation framework, leading to the incomplete performance evaluation for CC-SMPC compared with other methods. The analysis of the results for SMPC is mostly conducted with offline simulations or using only a limited number of online scenarios. However, the MPC mechanism for real-time operation management is based on the online scheme in practice, i.e., updating the EPS status and applying the optimized control strategy every time step. In addition, for time accumulated variables such as state of charge (SOC) of ESSs in SMPC, offline simulation is ineffective since

the uncertainty accumulates with time and leads to system divergence.

1.4. Contribution

In this paper, a CC-SMPC strategy is proposed to improve the performance of a novel modular-converter-based EPS with multiple ESSs on a MEA. This strategy is compatible with different EPS configurations. In addition to achieving multiple optimization objectives, the proposed CC-SMPC strategy is capable of coping with both normal and abnormal operating conditions. During the optimization, the CC-SMPC strategy simultaneously considers various uncertainty sources and multiple potential failures of system components. More specifically, this paper contributes to the following aspects:

1) It firstly proposes a DMPC strategy based on mixed-integer linear programming (MILP) for the novel multi-converter-based EPS on MEA. The goal is to minimize the power losses, the load shedding, and the switching activities in the system to avoid transients, and at the same time, maximize the energy stored in the ESSs. The EPS operation in both normal and faulty conditions is modeled by formulating several technical and operational constraints. These constraints are related to the: system configuration; bidirectionality of power flows; ESS; health status of system components; and potential failures.

2) A CC-SMPC model is proposed in the presence of uncertainty of load power demand on HV buses (HVBs) and LV buses (LVBs), again with potential failures. The probabilistic constraints on power limitations and ESS SOC are formulated based on the uncertainty propagations in the system, considering the power balance, components' health status, and system configuration. The proposed CC-SCMP model includes two main novelties. Firstly, different uncertainty sources are taken into account. The uncertainty on both HVBs and LVBs is studied in this paper, rather than focusing on the uncertainty of load power demand on a single bus. Secondly, the EPS configurations and power schedules are optimized for the minimum costs in both normal and faulty conditions under different uncertainty sources. In the meantime, the uncertainty can propagate differently in the system considering the interaction with the EPS configurations and power scheduling. These issues are addressed and formulated in the framework using mixed-integer quadratic programming (MIQP) optimization problems.

3) A comprehensive Monte-Carlo-based offline and online simulation is conducted for both DMPC and CC-SMPC methods, and the results are evaluated and compared using the proposed multi-dimensional evaluation framework. In this comparison, the multi-dimensional evaluation framework calculates operating costs, constraint violation costs, and total costs. In particular, instead of using a single index of average violation quantities, the constraint violation costs here consist of the average and maximum violation percentages and quantities.

The rest of this paper is organized as follows. The system configuration and the CC-SMPC controller framework are introduced in Section 2. Section 3 is dedicated to the mathematical formulation of the DMPC and modeling of the objective functions and constraints. In Section 4, the model presented in Section 3 is extended to CC-SMPC. In Section 5, simulation results for both DMPC and CC-SMPC methods are presented and evaluated for both normal and faulty operating conditions. The paper is concluded in Section 6.

2. System description and CC-SMPC framework

2.1. EPS description and assumptions

Fig. 1 presents a novel EPS architecture for an aircraft based on modular DC/DC power converters connecting the HV-side and LV-side
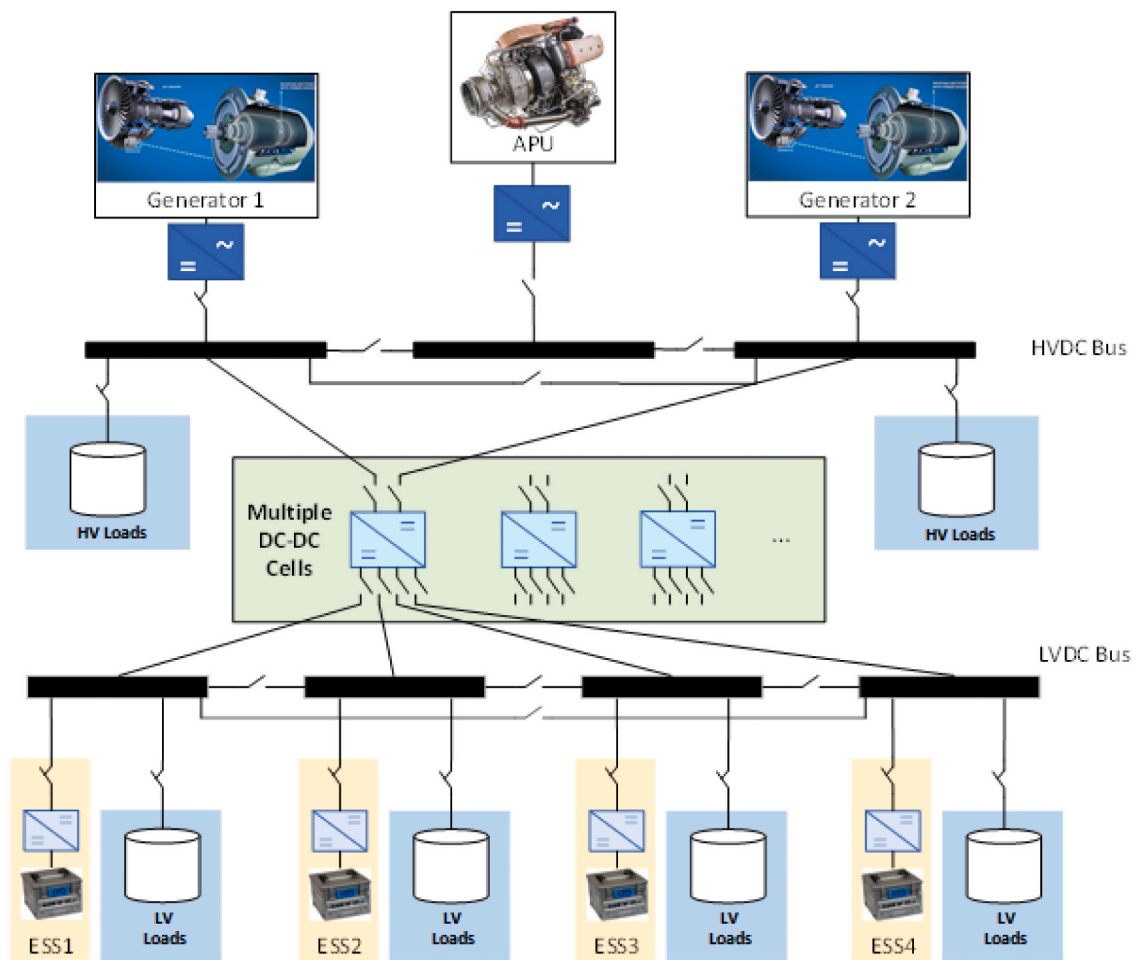
Fig. 1. A Novel EPS architecture for an aircraft based on modular converters and multiple ESSs.

of the system. In this architecture, two generators, with associated rectifiers, are connected to the corresponding HVDC buses, each of which supplies several HV loads. In addition, one auxiliary power unit (APU) is connected to the APU bus to support the system power demand under emergency conditions. For transferring power from the HV side to the LV side, several DC/DC power converters, called cells, can be connected to any HV/LV bus. Each LV bus is connected to an ESS comprised of one lithium-ion battery and one bidirectional DC/DC power converter, as well as several LV loads.

Two operating scenarios are considered for the EPS, namely the normal case and the faulty case, which are defined according to the health status of the EPS components. In the normal case, there is no failure in the system while in the faulty case, at least one of the system components is out of service. Accordingly, the role of the system components will change in different cases to ensure the power supply requirements of the HV/LV loads. A detailed description of the EPS components' roles is given in Table 2.

In an MEA system, the onboard loads usually change over time, according to different flight stages, including ground, take off, climb, cruise, descent, loiter, and landing [42]. The EPS loads include both critical loads and non-critical loads. The critical loads, such as flight control systems, essential environment control, and communication systems should be supplied in all scenarios. The non-critical loads can be shed, if needed, in failure scenarios which lead to a power shortage in the system. For the non-critical loads, load shedding can be conducted following load priorities, which means loads with higher priority are less preferred for load shedding. In this paper, the non-critical loads are classified into high priority loads (including the ice protection unit and

Table 2
EPS components' roles in normal and faulty operation cases.

EPS component	Normal case	Faulty case
Generators/ APU	The HV/LV loads are supplied by the two main generators. In addition, the generator output power is used to charge the batteries according to the ESS operating strategy.	In a generator failure scenario, the APU can be used to supply the loads. The APU starting time is assumed to be negligible.
ESS	The ESS is used to stabilize the LV bus voltage and help to compensate for the power deviations between the loads and the power transferred by cells.	ESSs can be used to supply LV loads when there is insufficient available power from the HV side, for instance in the case of failures in generators, transmission lines, and cells.
Transmission links	The LV buses are indirectly supplied by the generators, receiving power from HV buses via the transmission links. Each DC/DC cell can be connected to any HV or LV bus by controlling the on/off status of the contactors.	The multiple-cell architecture increases the flexibility and the reliability of the power transmission. For example, a failure in one contactor will not lead to the cell's unavailability for power transmission as the connections can be reconfigured to compensate for the failed contactor.

the sheddable parts of the environment control), mid priority loads (such as some galley loads), and low priority loads (such as lights and entertainment loads). Load prediction techniques can be deployed to

predict the aircraft load under different flight stages. In [43,44], online machine learning-based methods are adopted for load prediction in residential microgrid systems, which can be extended to be applied to MEA EPS by combining the updates with the flight stages, height, and historical data, which is the future study of the authors. In contrast, this paper, a simplified load prediction method is adopted in which load prediction is obtained by sampling the historical load without adjustment for real-time flight power changes.

This paper proposes a system-level operational management strategy for MEA based on the CC-SMPC strategy coping with the uncertainty in the aircraft power consumption at both HV and LV sides under normal and abnormal operating conditions. The following assumptions are considered for designing the CC-SMPC-based control strategy.

1) This paper concentrates on the system-level MPC controller to optimize the long-term performance of the system. The transient/short-term system behaviors are dealt with by another layer of control, which is beyond the scope of this paper.
2) The loads at both HV and LV sides are assumed to have underlying predictable components and uncertain deviations from these, which can be modeled by a normal probability distribution function (PDF), as shown in [32–34].
3) When a failure happens in a component, it is assumed that the component will not be recovered within the flight time. In addition, three types of component failures are considered in this work, including one generator failure, one ESS failure, and different transmission link failures including failures in contactors and cells.

2.2. Chance-constrained SMPC framework

Fig. 2 represents the proposed CC-SMPC-based control framework for controlling the system operation. As illustrated in the figure, at each time step k, the CC-SMPC-based control system receives the current status of the external system, to update the internal system state and constraints of the controller. An online optimization problem is solved with multi objectives to obtain an optimized control sequence for k, $k + 1$, ..., $k + N$-1, where N indicates the total time steps contained in the finite prediction horizon H. However, only the decisions for the first sample of the optimized control sequence are applied, and the horizon is shifted to the next time step $k + 1$.

As presented in Fig. 2, at each time step k, the load prediction $\mathbf{P}^{\text{Load}}(k, k + 1, ... N$-1) for the entire horizon is updated and sent to the controller, where $\mathbf{P}^{\text{Load}}$ indicates the matrix of predicted average and standard deviation (SD) values of all loads. In addition, based on the new measurements of the external system, received at the current time step, the internal system status is updated and shared with the controller. The

status information includes the failure status matrix $\boldsymbol{\gamma}$ consisting of all failures in the system, the connection status matrix $\mathbf{S}'$ consisting of the on/off status of all switches, and the **SOC** matrix consisting of SOC of all ESS. This information is used for updating the system dynamics and resetting the feasible region of the optimization problem included in the controller for the entire prediction horizon. After the optimization problem is solved, the CC-SMPC-based controller directly provides the reference values of the configuration/connection matrix **S** and power references of all cells $\mathbf{P}^{\text{Cell}}$ to the external system. Since the generators/APU and ESS are operated in voltage control mode, following the decided configurations, cells' power, and loads' power, other power flows in the system are determined based on Kirchhoff's Current Law.

3. Problem formulation of DMPC

As represented in Fig. 2, the MPC-based controller solves an online optimization problem over the prediction horizon at each step to find the optimal operating strategy considering the desired performance and system constraints. Hence, it is essential to formalize the system operation rules and targets in the form of a simplified mathematical model that can be efficiently solved. In this section, the proposed model for the conventional MPC is formulized in the MILP framework, which can be solved using available solvers, such as CPLEX and GUROBI at each time step.

3.1. Objective functions

For the optimal operational management of the EPS, the following four control targets are considered.

1) *Minimizing the total power from generators*: Reducing the total output power of the generators is the first control goal in our formulation because this indicates less fuel consumption for the flight. Since the generator power is used for supplying loads and charging batteries, reducing the power losses for these two power consumers is a key objective.

$$J_{PG} = \sum_{k=0}^{N-1} \frac{\sum_{j}^{N^{HVB}} P_j^G(k) + P^{APU}(k)}{N^G \bullet P^{Gmax}} \tag{1}$$

2) *Maximizing the energy stored in the ESS*: For ESS management, it is preferred to keep the aircraft battery at a high SOC value, within the target range, thereby being prepared for the abnormal conditions which may need the energy. To this aim, it is preferred to avoid
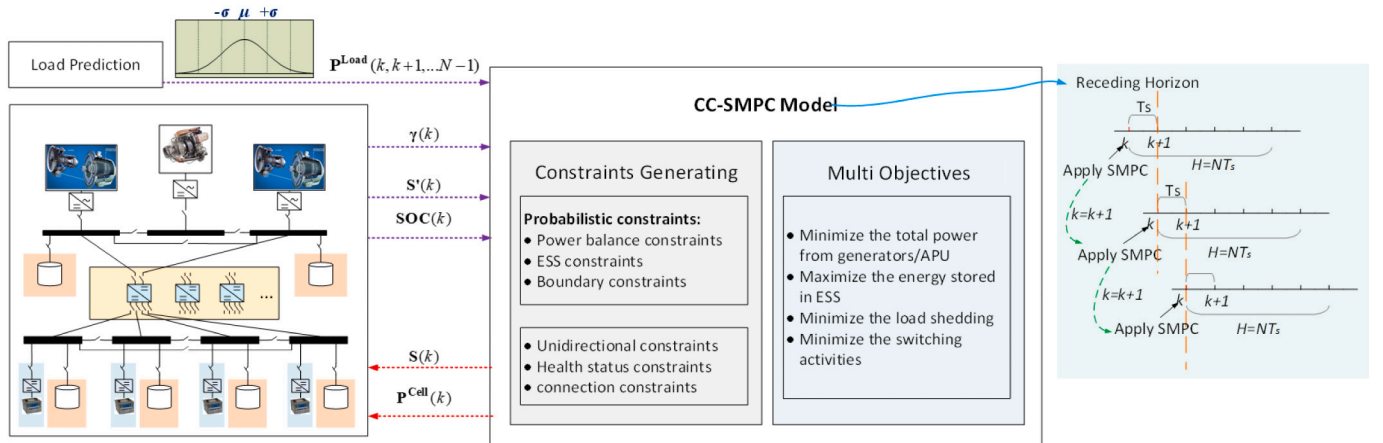

Fig. 2. Flowchart of the proposed online CC-SMPC optimization framework.

battery discharging, while battery charging is encouraged. The following cost function is therefore adopted for this target.

$$J_{Pbat} = \sum_{k=0}^{N-1} \frac{\sum_l^{N^{LVB}} - P_l^{bat}(k)}{N^G \bullet P_l^{batmax}} \qquad (2)$$

4) *Minimizing the switching activities*: Switching activities include the following changes: starting/stopping the APU, configuration changes in the transmission system (e.g. bus connections, cell connections,

$$J_{SL} = \sum_{k=0}^{N-1} \frac{\sum_j^{N^{HVB}} \sum_p^{N^{HVLncri}} \lambda_{jp}^{HVLncri} \left(- S_{jp}^{HVLncri}(k) \right) + \sum_l^{N^{LVB}} \sum_p^{N^{LVLncri}} \lambda_{jp}^{LVLncri} \left(- S_{jp}^{LVLncri}(k) \right)}{\sum_j^{N^{HVB}} \sum_p^{N^{HVLncri}} \lambda_{jp}^{HVLncri} + \sum_l^{N^{LVB}} \sum_p^{N^{LVLncri}} \lambda_{jp}^{LVLncri}} \qquad (3)$$

3) *Minimizing the load shedding*: In EPS normal flight scenarios, the power demand should be completely satisfied at all times, as generators are designed to supply the entire aircraft load. When the EPS is in a failure case, the power supply might be insufficient to support all of the non-critical loads. Therefore, load shedding of lower priority can be conducted to maintain safe system operation. The cost function in (3) is related to minimizing the total load shedding by penalizing the shedding of loads, considering load priorities.

etc.), and connecting/disconnecting loads. Switching activities are preferred to be avoided in the EPS of the aircraft as they might lead to unnecessary transients and can negatively affect the components' lifetimes. Cost functions (4)–(6) are adopted to minimize various types of switching activities, which are allocated with different appropriate weighting factors.

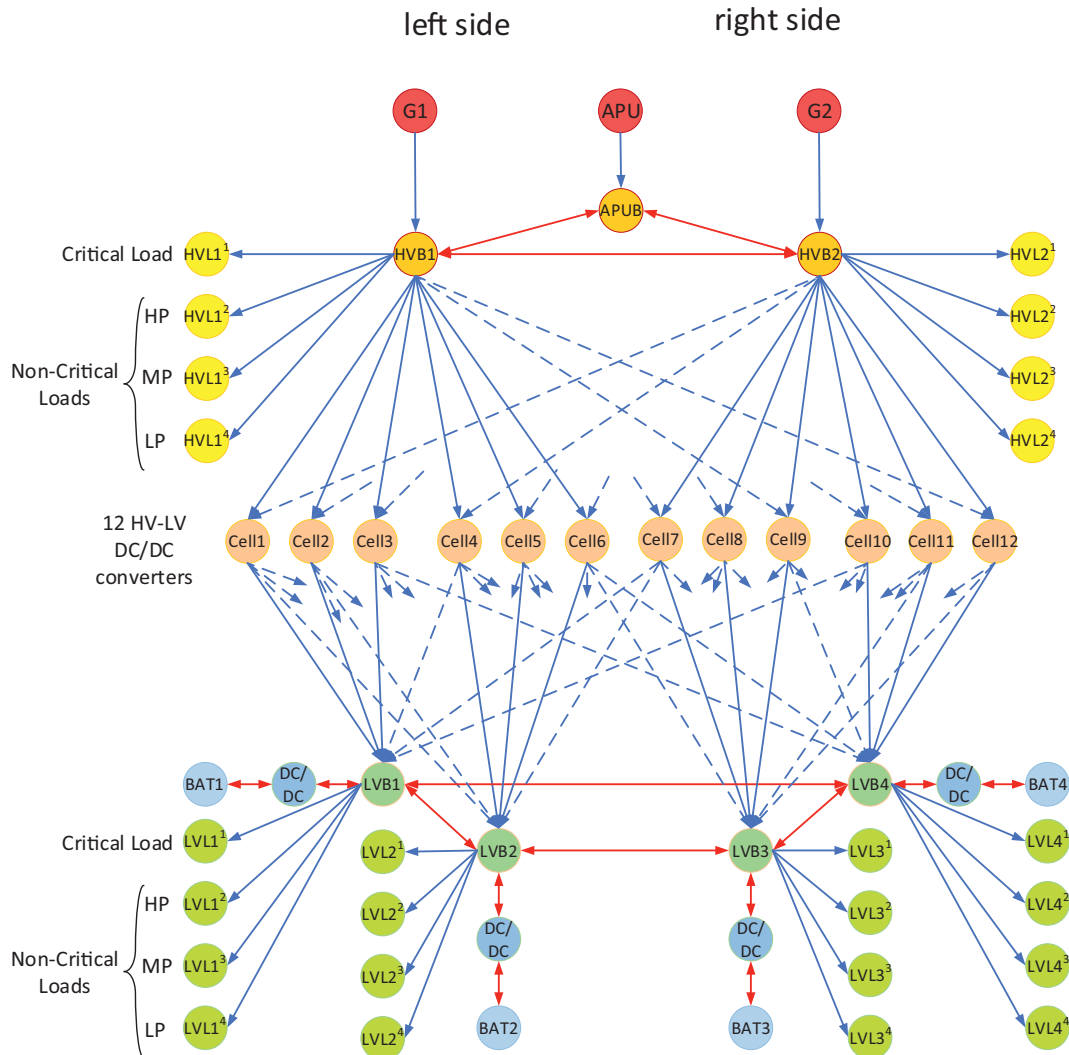$$J_{\delta APU} = \sum_{k=0}^{N-1} |S^{APU}(k+1) - S^{APU}(k)| \qquad (4)$$

Fig. 3. Power flow diagram of the novel EPS for MEA.

$$J_{\delta tran} = \sum_{k=0}^{N-1} \sum |S^{tran}(k+1) - S^{tran}(k)| \tag{5}$$

$$J_{\delta L} = \sum_{k=0}^{N-1} \sum |S^{L}(k+1) - S^{L}(k)| \tag{6}$$

where S^{tran} denotes the vector of all power transmission lines switches. Similarly, S^{L} denotes the vector of all load switches.

Finally, a multi-objective cost function is formed by combining all the cost functions introduced in (1)–(6) with different weighting factors w_{PG}, w_{Pbat}, w_{SL}, $w_{\delta APU}$, $w_{\delta tran}$, and $w_{\delta L}$ as follows.

$$Obj = w_{PG}J_{PG} + w_{Pbat}J_{Pbat} + w_{SL}J_{SL} + w_{\delta APU}J_{\delta APU} + w_{\delta tran}J_{\delta tran} + w_{\delta L}J_{\delta L} \tag{7}$$

3.2. Constraints

According to the system descriptions in Section 2, the system's operational and technical requirements can be described as a set of constraints, including the power balance, power direction, connection restrictions, and battery dynamics. To better represent the potential power flow in the system, the power flow diagram in Fig. 3 is extracted from the system architecture shown in Fig. 1. System buses and components, such as generators, converters, batteries, and loads, are demonstrated as nodes. The potential power flows are demonstrated by lines with arrows, which show the direction of the power flow. The blue arrows demonstrate the unidirectional power flow, while the red arrows represent the bidirectional power flow.

3.2.1. Power balance constraints

For each bus node in Fig. 3, the power flow should comply with Kirchhoff's Current Law for a given voltage [45], assuming no losses within the bus itself. For the converter nodes, the power flowing out of each node is less than the power flowing into it because of the converter efficiency. In addition, power losses across the transmission lines are considered by adding a transmission efficiency parameter to the model.

1) Power balance for APU bus node: As represented in Fig. 3, the power from the APU is unidirectional, while the power from/to HV buses is bidirectional. The power flow in each direction is represented by a non-negative variable, hence the power balance equation can be written as follows:

$$P^{APU}(k) - \sum_{j}^{N^{HVB}} P_j^{AHVp}(k) + \sum_{j}^{N^{HVB}} \eta_j^{AHV} P_j^{AHVn}(k) = 0 \tag{8}$$

According to (8), the total power flowing from the APU and HV buses to the APU bus should be equal to the power that flows from APU bus to the HV buses.

2) Power balance for HV bus nodes: The input power for an HV bus includes the power from a generator, APU bus, and adjacent HV buses, while the output power includes the power to HV loads, cells, and adjacent HV buses as follows. Accordingly, the first three terms in (9) indicate the input power for an HV bus, while the following three terms indicate the output power.

$$P_j^G(k) + \left(\eta_j^{AHV} P_j^{AHVp}(k) - P_j^{AHVn}(k)\right) + \left(\sum_{j \neq j'} \left(\eta_{jj'}^{HV} P_{j'j}^{HV}(k) - P_{jj'}^{HV}(k)\right)\right)$$
$$- \sum_{c}^{N^C} P_{jc}^{HVC}(k) - \sum_{p}^{N^{HVLcri}} P_{jp}^{HVLcri}(k) - \sum_{p}^{N^{HVLncri}} S_{jp}^{HVLncri}(k)P_{jp}^{HVLncri}(k) = 0 \tag{9}$$

3) Power balance for cells' nodes: The cells operate in buck mode to transfer power from the HV side to the LV side, and the output power of each cell is less than its input power considering the power losses in the nodes (converter efficiency). This is presented in the following equation in which the first term is related to power flowing from HV

buses to a DC/DC converter and the second term shows the power flowing from the DC/DC converter to LV buss.

$$\eta_c \sum_{j}^{N^{HVB}} \eta_{jc}^{HVC} P_{jc}^{HVC}(k) - \sum_{l}^{N^{LVB}} P_{cl}^{LVC}(k) = 0 \tag{10}$$

Power balance for LV bus nodes: For each LV bus, the battery operates in voltage control mode to maintain the voltage constant. Therefore, the power of the battery is determined by the power of the cells, adjacent LV buses, and LV critical and non-critical loads. The following equation shows the power balance for LV bus l.

$$\sum_{c}^{N^C} \eta_{cl}^{LVC} P_{cl}^{LVC}(k) + \sum_{l \neq l'} \left(\eta_{ll'}^{LV} P_{l'l}^{LV}(k) - P_{ll'}^{LV}(k)\right) - P_l^{BAT}(k)$$
$$- \sum_{q}^{N^{LVLcri}} P_{lq}^{LVLcri}(k) - \sum_{q}^{N^{LVLncri}} S_{lq}^{LVLncri}(k)P_{lq}^{LVLncri}(k) = 0 \tag{11}$$

In (11), η_{cl}^{LVC} and $\eta_{ll'}^{LV}$ represent the transmission efficiency of cables between the DC/DC converters and LV buses and transmission efficiency in LV cables between buses l and l', respectively.

3.2.2. ESS constraints

The SOC of the batteries is related to the energy stored in a system [46]. For each battery, the SOC at time step $k + 1$ can be estimated from the battery power and SOC value at the previous time step k, as shown below. η_l^{BAT} indicates the charging/discharging efficiency of the battery, which is related to the battery power [46], [47].

$$SOC_l(k+1) = SOC_l(k) + T_s \eta_l^{BAT} P_l^{BAT}(k) / B_l^{cap} \tag{12}$$

In (12), $P_l^{BAT}(k)$ represents the battery power, which is assumed to be positive/negative during charging/discharging, respectively. Battery $SOC \in [0,1]$, where $SOC = 1$ indicates a fully charged battery, while $SOC = 0$ corresponds to a depleted battery. In the aircraft system, SOC is preferred to be kept within a target range [LO, HI] following operational requirements. Therefore, the upper and lower bounds are defined in (13), where LO = 0.3 and HI = 0.9 are considered in this study, which can be presented as ESS constraints in the optimization problem.

$$LO \leq SOC_l(k) \leq HI \tag{13}$$

3.2.3. Boundary constraints

Each component and transmission link has its maximum power limitation for safe operation. For the potential unidirectional power flow, when its physical transmission path is connected, the power should not exceed its limits. Otherwise, the power is restricted to 0. Similarly, for the potential bidirectional power flow in bus interconnections, the power is limited by the direction indicator, i.e. only the selected power direction can reach its maximum power limitation. This set of constraints is presented below.

$$S(k) \times P_{min} \leq P(k) \leq S(k) \times P_{max} \tag{14}$$

where $P(k)$ denotes the vector of power flow variables, and $S(k)$ denotes the vector of binary variables of physical connections and power flow direction indicators. In (14), P_{max} and P_{min} denote the vector of the corresponding power limitations.

3.2.4. Unidirectional constraints

For the potential bidirectional power flow in bus interconnections, two non-negative variables are introduced to present the power flow in each direction separately. The unidirectional constraints in (15) combined with (14) are used to avoid power flow in both directions simultaneously. Eqs. (15) and (14) indicate that when the physical transmission link is connected, the power can be transferred in one of the directions with the given maximum value while the maximum power in the opposite direction is restricted to 0. When the physical transmission link is disconnected, power flow in both directions is set to zero. More modeling details and examples for boundary and unidirectional

constraints are discussed in our previous study in [48].

$$s^p(k) + s^n(k) \leq S^{Phy}(k) \tag{15}$$

In (15), $s^p(k)$ and $s^n(k)$ are vectors of binary variables that denote positive and negative direction indicators respectively. For example, $s^p(k)$ includes the direction indicator $s_j^{AHVp}(k)$, $s_{jj}^{HV}(k)$, and $s_{ll}^{LV}(k)$, while $s^n(k)$ includes the direction indicator $s_j^{AHVn}(k)$, $s_{j'j}^{HV}(k)$, and $s_{l'l}^{LY}(k)$. In addition, $S^{Phy}(k)$ is the vector of their corresponding physical connections.

3.2.5. Health status constraints

As mentioned in Section 2, several failure scenarios for system components such as generators, ESS, and cells, are considered in this study. To force the MPC controller to cope with the failure scenarios, the health status constraints in (16) are taken into account. These constraints indicate that the components can be connected when they are in the normal condition; otherwise, they will be forcibly disconnected in the case of failure.

$$S^h(k) \leq \gamma(k) \tag{16}$$

Where $S^h(k)$ denotes the vectors of connections status and $\gamma(k)$ denotes the failure status matrix consisting of all failures in the system.

3.2.6. Operational connection constraints

The power contactors should be connected properly to provide the system with all possible operation topologies and prevent unexpected connection conditions. The connection constraints are proposed mainly for APU connection, interconnection of buses, and the cells' connections as follows.

1) In the generators' normal condition, APU is not used. In contrast, when any of the main generators fails, APU can be connected to the APU bus to further supply the HV buses:

$$S^{APU}(k) \leq \left(1 - \prod_j^{N^{HVB}} \gamma_j^G(k)\right) \tag{17}$$

In (17), the multiplication operator in the right-hand side means that in case all generators are in healthy situation ($\gamma_j^G(k) = 1$), connection of APU to the system is not allowed.

2) The HV bus interconnections are only allowed when any generator failure occurs. This is to stabilize the HV bus voltage and maintain critical HV loads. Besides, HV buses should be connected without creating loops:

$$\sum_j^{N^{HVB}} S_j^{AHV}(k) + S_{jj'}^{HV}(k) \leq N^{HVB} \bullet \left(1 - \prod_{j'}^{N^{HVB}} \gamma_i^G(k)\right) \tag{18}$$

$$\sum_j^{N^{HVB}} S_j^G(k) + S^{APU}(k) + \sum_j^{N^{HVB}} S_j^{AHV}(k) + S_{jj'}^{HV}(k) \leq N^{HVB} + N^{APU} \tag{19}$$

As presented in (18), if all values of $\gamma_i^G(k^{HL})$ are 1, no HV/APU bus interconnection is allowed; otherwise, the maximum number of N^{HVB} bus interconnections can be adopted to connect the HV and APU buses. In addition, to avoid the loop, the number of faulty generators indicates the maximum number of bus interconnections required, as presented in (19).

3) Each HV bus should be supplied by only one healthy power source, either one main generator or the APU, which is combined with constraints in (18)–(19):

$$1 \leq S_j^G(k) + S_j^{AHV}(k) + S_{jj'}^{HV}(k) \leq 2 \tag{20}$$

As presented in (20), if $S_j^G(k^{HL}) = 0$, indicating a faulty generator j, then at least one bus interconnection (any of $S_j^{AHV}(k^{HL})$ and $S_{jj'}^{HV}(k^{HL})$)

will be adopted to supply the HV bus j.

4) Although the cells are flexible to be connected with any HV/LV bus, during the system operation, one cell cannot be connected with more than one HV and LV bus. These constraints are modeled by following equations:

$$0 \leq \sum_j^{N^{HVB}} S_{jc}^{HVC}(k) \leq 1 \tag{21}$$

$$0 \leq \sum_l^{N^{LVB}} S_{cl}^{LVC}(k) \leq 1 \tag{22}$$

5) The LV bus interconnections are only allowed when a battery failure occurs. This is to stabilize the LV bus voltage and maintain critical LV loads. LV buses should be connected without creating loops:

$$\sum_l^{N^{LVB}} S_{ll'}^{LV}(k) \leq \left(N^{BAT} - 1\right)\left(1 - \prod_j^{N^{HVB}} \gamma_l^{BAT}(k)\right) \tag{23}$$

$$\sum_l^{N^{LVB}} S_l^{BAT}(k) + \sum_l^{N^{LVB}} S_{ll'}^{LY}(k) \leq N^{BAT} \tag{24}$$

In (23), the multiplication operator in the second term of the right-hand side means that when all batteries are in a healthy situation ($\forall l \in \{1, ..., N^{LVB}\}$,), LV bus interconnection is not allowed. Otherwise, a maximum number of $N^{BAT} - 1$ bus interconnections can be adopted, to connect the N^{BAT} LV buses. In addition, the number of faulty batteries indicates the maximum number of LV bus interconnections required to compensate, as presented in (24).

6) Each LV bus should be supplied with only one healthy battery, which is combined with constraints in (23)–(24):

$$S_l^{BAT}(k) + S_{l(l-1)}^{LV}(k) + S_{l(l+1)}^{LV}(k) \geq 1 \tag{25}$$

As presented in (25), if $S_l^{BAT}(k) = 0$, indicating a faulty battery l, then at least one LV bus interconnection will need to be adopted to supply the LV bus l.

4. Chance-constrained model predictive control

In the DMPC model discussed in Section 3, the power consumption of loads at both HV and LV sides is assumed to be equal to the predicted values without any deviations. However, uncertainty is an inseparable part of real systems and load forecasting is quite likely to be imperfect. Moreover, although most of the MEA loads are predictable, it is difficult to precisely predict the power consumption behavior of all parts of the system. This uncertainty in the system can lead to performance degradation of the conventional MPC methods that are based on the certainty equivalence principle. Hence, to overcome this limitation and explicitly take into account the uncertain nature of random parameters, CC-SMPC is used. In CC-SMPC, constraints with random variables are replaced with probabilistic constraints, which means instead of guaranteeing the satisfaction of system constraints at all time instances, it is guaranteed that the probability of satisfying the probabilistic constraints is higher than a pre-specified confidence level.

In this study, the CC-SMPC model is developed taking into account the load uncertainty at both HV and LV sides. Furthermore, multiple failures in generators, batteries, and transmission links from HV buses to LV buses are considered (e.g. failures in cells). This leads to the change of the model from a MILP problem to a Mixed-Integer Nonlinear Programming (MINLP) problem. Since solving an optimization problem with probabilistic constraints is a difficult task, probabilistic constraints are replaced with their deterministic counterparts using the probability distribution knowledge of the uncertain parameters. It should be mentioned that the proposed model is applicable for the EPS management in both normal and faulty scenarios.

4.1. Uncertainty on the HV side with potential failures

Due to the forecasting errors, loads are commonly described with a Gaussian PDF with its mean value equal to the forecasted load [49]. In this study, Gaussian PDFs in (26) and (27) are assumed to represent the uncertainty of power demands of the HV loads, with mean values of $\overline{P}_{jp}^{HVLcri}$ and $\overline{P}_{jp}^{HVLncri}$ and SDs of $\sigma_{P_{jp}^{HVLcri}}$ and $\sigma_{P_{jp}^{HVLncri}}$, for critical and non-critical loads, respectively.

$$P_{jp}^{HVLcri}(k) = \mathscr{DN}\left(\overline{P}_{jp}^{HVLcri}(k), \sigma_{P_{jp}^{HVLcri}}(k)\right) \tag{26}$$

$$P_{jp}^{HVLncri}(k) = \mathscr{DN}\left(\overline{P}_{jp}^{HVLncri}(k), \sigma_{P_{jp}^{HVLncri}}(k)\right) \tag{27}$$

It should be mentioned that the uncertainty in each HV load affects only the associated HV bus and is compensated for by the generators/APU, while the power transferred to the cells is deterministic. This assumption is reasonable as generators and APU operate in the voltage control mode to compensate for the uncertainty, within their power capacity. Therefore, following the uncertainty propagation calculation rules in [50], the mean value of the generator power and the power of the HV interconnection buses is calculated according to (28). The SD of the generator output power is calculated using (29). The formulation indicates that when one generator is in a faulty condition, the other generator is required to compensate for load uncertainties on both HV buses if the buses are connected. Otherwise, if the HV buses are not connected, the generator in the normal condition only compensates for

In the case of generator failure, the APU can be connected to the system to replace the failed generator. Similar to the formulations in (28) and (29), the mean value of the APU output power is calculated using (30), which is based on (8). According to (28), the APU only compensates for the HV load uncertainties when it is connected to one failed bus, hence the SD value is calculated by (31).

$$\overline{P}^{APU}(k) = \sum_{j}^{N^{HVB}} \overline{P}_{j}^{AHVp}(k) - \sum_{j}^{N^{HVB}} \eta_{j}^{AHV}\overline{P}_{j}^{AHVn}(k) \tag{30}$$

Since the generator/APU output power is uncertain, the deterministic boundary constraints for its power limitation in (14) need to be replaced with the two probabilistic constraints introduced in (32), where ρ_{j}^{Pg} indicates the probability for the boundary violation. By adopting the linearization methods in [51], the probabilistic constraints in (32) are linearized using (33) and (34) for generators and APU respectively, where $\sigma_{P_{j}^G}^2(k)$ is calculated by (29), and $\sigma_{P_{APU}}^2(k)$ is calculated by (31). In (33) and (34), erf^{-1} is the inverse error function.

$$Pr\left(-P_{j}^{Gmax} \leq P_{j}^{G,APU}(k) \leq P_{j}^{Gmax}\right) \geq 1 - \rho_{j}^{Pg} \tag{32}$$

$$\sigma_{P_{j}^G}^2(k) = \gamma_j^G(k) \bullet \left(\begin{array}{c} \left(\sum_p^{N^{HVLcri}} \sigma_{P_{jp}^{HVLcri}}^2(k) + \sum_p^{N^{HVLncri}} S_{jp}^{HVLncri}(k)\sigma_{P_{jp}^{HVLncri}}^2(k)\right) \\ \\ +\dfrac{S^{HV}(k)}{\eta^{HV2}}\left(\sum_p^{N^{HVLcri}} \sigma_{P_{j'p}^{HVLcri}}^2(k) + \sum_p^{N^{HVLncri}} S_{j'p}^{HVLncri}(k)\sigma_{P_{j'p}^{HVLncri}}^2(k)\right) \\ \\ +\dfrac{1-S^{APU}(k)}{\left(\prod_j^{N^{HVB}} \eta_j^{AHV}\right)^2}\left(\sum_p^{N^{HVLcri}} \sigma_{P_{j'p}^{HVLcri}}^2(k) + \sum_p^{N^{HVLncri}} S_{j'p}^{HVLncri}(k)\sigma_{P_{j'p}^{HVLncri}}^2(k)\right) \end{array} \right) \tag{29}$$

the load uncertainties on its corresponding HV bus. Moreover, the generator in the faulty condition should be removed from the uncertainty propagation model.

$$\overline{P}_{j}^{G}(k) + \left(\eta_{j}^{AHV}\overline{P}_{j}^{AHVp}(k) - \overline{P}_{j}^{AHVn}(k)\right) + \left(\sum_{j \neq j'}\left(\eta_{jj'}^{HV}\overline{P}_{j'j}^{HV}(k) - \overline{P}_{jj'}^{HV}(k)\right)\right)$$
$$= \sum_{c}^{N^C} P_{jc}^{HVC}(k) + \sum_{p}^{N^{HVLcri}} \overline{P}_{jp}^{HVLcri}(k) - \sum_{p}^{N^{HVLncri}} S_{jp}^{HVLncri}(k)\overline{P}_{jp}^{HVLncri}(k) \tag{28}$$

$$-P_{j}^{Gmax} + \sqrt{2}\sigma_{P_{j}^G}(k)erf^{-1}\left(1 - 2\rho_{j}^{Pg}\right) \leq \overline{P}_{j}^{G}(k)$$
$$\leq P_{j}^{Gmax} - \sqrt{2}\sigma_{P_{j}^G}(k)erf^{-1}\left(1 - 2\rho_{j}^{Pg}\right) \tag{33}$$

$$-P_{j}^{Gmax} + \sqrt{2}\sigma_{P_{APU}}(k)erf^{-1}\left(1 - 2\rho_{j}^{Pg}\right) \leq \overline{P}^{APU}(k)$$
$$\leq P_{j}^{Gmax} - \sqrt{2}\sigma_{P_{APU}}(k)erf^{-1}\left(1 - 2\rho_{j}^{Pg}\right) \tag{34}$$

$$\sigma_{P_{APU}}^2(k) = S^{APU} \bullet \left(\begin{array}{c} \dfrac{1-\gamma_j^G(k)}{\eta_j^{AHV2}}\left(\sum_p^{N^{HVLcri}} \sigma_{P_{jp}^{HVLcri}}^2(k) + \sum_p^{N^{HVLncri}} S_{jp}^{HVLncri}(k)\sigma_{P_{jp}^{HVLncri}}^2(k)\right) \\ \\ +\dfrac{1-\gamma_j^G(k)}{\eta_{j'}^{AHV2}}\left(\sum_p^{N^{HVLcri}} \sigma_{P_{j'p}^{HVLcri}}^2(k) + \sum_p^{N^{HVLncri}} S_{j'p}^{HVLncri}(k)\sigma_{P_{j'p}^{HVLncri}}^2(k)\right) \end{array} \right) \tag{31}$$

4.2. Uncertainty on the LV side with potential failures

Similarly to the HV side uncertainty analysis, the uncertain parameters of the LV loads are assumed to follow a Gaussian PDF, with the mean value of $\overline{P}_{lq}^{LVLcri}$ and $\overline{P}_{lq}^{LVLncri}$ and SD of $\sigma_{P_{lq}^{LVLcri}}$ and $\sigma_{P_{lq}^{LVLncri}}$, for critical and non-critical loads, respectively, as shown in (35) and (36).

$$P_{lq}^{LVLcri}(k) = \mathscr{DN}\left(\overline{P}_{lq}^{LVLcri}(k), \sigma_{P_{lq}^{LVLcri}}(k)\right) \tag{35}$$

$$P_{lq}^{LVLncri}(k) = \mathscr{DN}\left(\overline{P}_{lq}^{LVLncri}(k), \sigma_{P_{lq}^{LVLncri}}(k)\right) \tag{36}$$

Since the power transferred to the cells is deterministic, batteries are used to compensate for the LV loads' uncertainty. In a normal operation scenario, the LV buses will not be interconnected (according to con-

$$\sigma_{P_l^{BAT}}^2(k) = \gamma_j^{BAT} \bullet \left(\begin{array}{c} \left(\sum_q^{N^{LVLcri}} \sigma_{P_{lq}^{LVLcri}}^2(k) + \sum_q^{N^{LVLncri}} S_{lq}^{LVLncri}(k)\sigma_{P_{lq}^{LVLncri}}^2(k)\right) \\ + \dfrac{S_{l+1}^{LV}}{\eta_{l(l+1)}^{LV\,2}}\left(\sum_q^{N^{LVLcri}} \sigma_{P_{(l+1)q}^{LVLcri}}^2(k) + \sum_q^{N^{LVLncri}} S_{(l+1)q}^{LVLncri}(k)\sigma_{P_{(l+1)q}^{LVLncri}}^2(k)\right) \\ + \dfrac{S_{l-1}^{LV}}{\eta_{l(l-1)}^{LV\,2}}\left(\sum_q^{N^{LVLcri}} \sigma_{P_{(l-1)q}^{LVLcri}}^2(k) + \sum_q^{N^{LVLncri}} S_{(l-1)q}^{LVLncri}(k)\sigma_{P_{(l-1)q}^{LVLncri}}^2(k)\right) \end{array} \right) \tag{38}$$

straints (23)–(24)), and the LV loads' uncertainty for each LV bus is independent of that of adjacent LV buses. When one battery fails, the LV bus interconnection is required to maintain the bus voltage, using an adjacent healthy battery. Consequently, the connected adjacent battery will also compensate for the load uncertainties on the connected LV buses. Based on the power balance equation in (11), the mean and SD ($\sigma_{P_l^{BAT}}(k)$) values of the batteries' power are calculated using (37) and (38), respectively, taking into account the uncertain load power propagation from the adjacent LV bus node.

$$\overline{P}_l^{BAT}(k) = \sum_c^{N^C} \eta_{cl}^{LVC}P_{cl}^{LVC}(k) + \sum_{l\neq l'}\left(\eta_{ll'}^{LV}P_{l'l}^{LV}(k) - P_{ll'}^{LV}(k)\right)$$
$$- \sum_q^{N^{LVLcri}}\overline{P}_{lq}^{LVLcri}(k) - \sum_q^{N^{LVLncri}} S_{lq}^{LVLncri}(k)\overline{P}_{lq}^{LVLncri}(k) \tag{37}$$

Since the battery charge level is dependent on the integration of the battery power over time, the uncertain battery power will lead to a nondeterministic battery charge level. According to the battery SOC dynamic equation in (12), the mean and SD values of SOC can be calculated by (39) and (40), respectively.

$$\overline{SOC_l}(k+1) = \overline{SOC_l}(k) + \frac{\overline{P}_l^{BAT}(k)}{B_l^{cap}}T_s\eta_l^{BAT} \tag{39}$$

$$\sigma_{SOC_l}^2(k+1) = \sigma_{SOC_l}^2(k) + \left(T_s\eta_l^{BAT}\right)^2\sigma_{P_l^{BAT}}^2(k)\Big/B_l^{cap\,2} \tag{40}$$

Accordingly, the constraints related to the SOC target range (13) as well as the boundary constraints of the battery power (14) are replaced with probabilistic constraints in (41)–(42). Satisfying the probabilistic constraints ensures that the probability of not violating the constraints will be higher than a pre-specified confidence level corresponding to constraint violations of ρ_l^{SOC} and ρ_l^{Pbat}.

$$Pr\left(LO \leq SOC_l(k+1) \leq HI\right) \geq 1 - \rho_l^{SOC} \tag{41}$$

$$Pr\left(-P_l^{batmax} \leq P_l^{BAT}(k) \leq P_l^{batmax}\right) \geq 1 - \rho_l^{Pbat} \tag{42}$$

By adopting linearization methods in [51], the probabilistic constraints can be replaced with two deterministic inequality constraints using the mean and SD values as shown in (43) and (44).

$$-P_l^{batmax} + \sqrt{2}\sigma_{P_l^{BAT}}(k)erf^{-1}\left(1-2\rho_l^{Pbat}\right) \leq \overline{P}_l^{BAT}(k)$$
$$\leq P_l^{batmax} - \sqrt{2}\sigma_{P_l^{BAT}}(k)erf^{-1}\left(1-2\rho_l^{Pbat}\right) \tag{43}$$

$$LO + \sqrt{2}\sigma_{SOC_l}(k+1)erf^{-1}\left(1-2\rho_l^{SOC}\right) \leq \overline{SOC_l}(k+1)$$
$$\leq HI - \sqrt{2}\sigma_{SOC_l}(k+1)erf^{-1}\left(1-2\rho_l^{SOC}\right) \tag{44}$$

The complete CC-SMPC model includes the constraints in (8)–(25) as well as constraints (35)–(44). The objective function is similar to the DMPC model in (1)–(7), where the uncertain variables are replaced with their mean values.

5. Simulation results

In this section, simulation results of system operation are evaluated and compared for two cases, i.e. the normal case, and the faulty case, when adopting the proposed CC-SMPC and the DMPC strategies. For each case, both offline (single independent evaluations) and online (evaluation within a receding horizon approach) comparison results are presented and analyzed. For the offline test, the CC-SMPC and DMPC strategies are applied to the system for a flight duration of $T = 150$ min, considering the forecasted loads of the system at both the HV and LV sides. Afterwards, the performance of both control strategies is evaluated under the realization of a large number of random load scenarios. The offline results provide quick verification for the CC-SMPC for power limitation violation analysis as the offline tests are quicker to execute and hundreds of load scenarios can be considered. However, offline testing is not applicable for the assessment of SOC violation and costs of system operation, because the SOC is a time accumulating variable. Therefore, offline testing leads to accumulating SOC deviations due to the lack of ability to take corrective actions. In contrast, online testing is applicable for the evaluation of all violation analyses and the real cost of system operation. However, the computational time is considerably increased for testing hundreds of load scenarios. Hence, for the offline tests, 100 uncertain load profiles are tested in which the maximum acceptable probability of constraint violations varies from 0.01 to 0.2, to verify the feasibility of the model. In the second step, the online DMPC and CC-SMPC techniques are applied for 50 uncertain load profiles with a selected probability, which compares the total cost of system operation and the penalty costs of constraint violations.

5.1. Introduction of the evaluation framework

The predicted load profile (mean value of each load's power) in Fig. 3 is presented in Table 6 in Appendix A. The maximum load power is 95 kW when the aircraft enters the cruising stage, while the rated generator

power is 97 kW, which is designed to cover all of the MEA loads. The rated power for each DC/DC converter is 3 kW, and the battery capacity of all batteries is 4kWh.

For comparing the online DMPC and CC-SMPC performance, an evaluation framework for comparing the system operation costs and constraint violation costs is proposed in the following, which evaluates the system performance for $N^{Scen} = 50$ load scenarios over the whole flight duration $T = 150$ min. The operation costs are calculated based on the controller objectives, which contain power losses, stored energy, load shedding, and switching activities.

The power loss for each single time step of each testing scenario equals the difference between the total supplied power in (45) and the total load power (47). The power losses for all of the scenarios during the entire flight are evaluated by (45), calculating the average power loss, which is weighted by the weighting factor v_{Ploss}.

$$Q_{Ploss} = v_{Ploss}\left(\frac{1}{N^{Scen}T}\sum\nolimits_{n=1}^{N^{Scen}}\sum\nolimits_{k=0}^{T}\left(P_n^{source}(k) - P_n^{load}(k)\right)\right) \quad (45)$$

$$P_n^{source}(k) = \sum\nolimits_{j}^{N^{HVB}}P_j^G(k) + P^{APU}(k) - \eta_l^{BAT}\sum\nolimits_{l}^{N^{LVB}}P_l^{BAT}(k) \quad (46)$$

$$P_n^{load}(k) = \sum\nolimits_{p}^{N^{HVLcri}}P_{jp}^{HVLcri}(k) + \sum\nolimits_{p}^{N^{HVLncri}}S_{jp}^{HVLncri}(k)P_{jp}^{HVLncri}(k)$$
$$+ \sum\nolimits_{q}^{N^{LVLcri}}P_{lq}^{LVLcri}(k) + \sum\nolimits_{q}^{N^{LVLncri}}S_{lq}^{LVLncri}(k)P_{lq}^{LVLncri}(k)\right) \quad (47)$$

The ESS performance is evaluated by SOC level in (48) for all load scenarios, which indicates that a better performance for the SOC average value is one that is closer to the upper bound within the target range.

$$Q_{SOC} = v_{SOC}\left(\frac{1}{N^{Scen}T}\sum\nolimits_{n=1}^{N^{Scen}}\sum\nolimits_{k=0}^{T}\sum\nolimits_{l}^{N^{BAT}}|HI - SOC_{n,l}(k)|\right) \quad (48)$$

The performances for load shedding and switching activities are evaluated by similar methods, which are used in calculating the objective functions (3)–(6), considering the entire flight duration. Based on this, the load shedding and switching activity evaluations for all test scenarios are conducted by calculating the average load shedding for each scenario using (49) and the average switching activities using (50), with v_{SL}, $v_{\delta APU}$, $v_{\delta tran}$, and $v_{\delta L}$ being the weighting factors for the relative importance of load shedding (J_{SL}), starting/stopping the APU ($J_{\delta APU}$),

configuration changes in the transmission system ($J_{\delta tran}$), and loads on/off status ($J_{\delta L}$), respectively.

$$Q_{SL} = v_{SL}\frac{1}{N^{Scen}T}\sum\nolimits_{n=1}^{N^{Scen}}J_{SL} \quad (49)$$

$$Q_\delta = \frac{1}{N^{Scen}T}\left(v_{\delta APU}\sum\nolimits_{n=1}^{N^{Scen}}J_{\delta APU} + v_{\delta tran}\sum\nolimits_{n=1}^{N^{Scen}}J_{\delta tran} + v_{\delta L}\sum\nolimits_{n=1}^{N^{Scen}}J_{\delta L}\right) \quad (50)$$

As demonstrated in Section 4, the uncertainty in the system can lead to potential violations of three constraints, including the violation of SOC target range, the violation of maximum power bounds for batteries, and the violation of maximum power bounds for generator/APU output power. To better evaluate the violation cost, instead of using only one average value or maximum value, a new index is proposed that combines four dimensions. The violation cost is calculated based on the maximum percentage of constraint violation in all scenarios over all time steps (Q_{*mp}'), the average percentage of constraint violation over all time steps with violation occurrence (Q_{*ap}'), the maximum constraint violation value (Q_{*mq}'), and the average constraint violation value across all time steps with violation occurrence and scenarios (Q_{*aq}'). For example, (51)–(54) are adopted for the SOC violation cost based on the aforementioned evaluation scheme, and the overall cost is calculated by their combination with weights presented in (55). In this work, it is assumed that each type of violation is weighted equally, which indicates that $v_{SOCmp} = v_{SOCap} = v_{SOCmq} = v_{SOCap} = 0.25$. Similarly, the violation

$$Q_{SOCaq}' = \frac{\sum\left\{SOC_{n,l}(k) \in S:\left(SOC_{n,l}(k) > HI \vee SOC_{n,l}(k) < LO\right)\right\}\left(|SOC_{n,l}(k) - HI| + |SOC_{n,l}(k) - LO|\right)}{\sum\left\{n \in S:\left(SOC_{n,l}(k) > HI \vee SOC_{n,l}(k) < LO\right)\right\}} \quad (54)$$

cost for battery power Q_{Pbat}' (including Q_{Pbatmp}', Q_{Pbatap}', Q_{Pbatmq}', Q_{Pbataq}') and generator/APU output power Q_{Pgen}' (including Q_{Pgenmp}', Q_{Pgenap}', Q_{Pgenmq}', Q_{Pgenaq}') can be calculated by the same method (for the sake of brevity, detailed functions are omitted).

$$Q_{SOCmp}' = \frac{max\left\{n : n \in S:\left(SOC_{n,l}(k) > HI \vee SOC_{n,l}(k) < LO\right)\right.}{N^{Scen}}, k$$
$$\in \{1, 2, ..., T\}\right\} \quad (51)$$

$$Q_{SOCap}' = \frac{\sum\left\{n \in S:\left(SOC_{n,l}(k) > HI \vee SOC_{n,l}(k) < LO\right)\right\}}{N^{Scen}\sum\left\{k \in S:\left(SOC_{n,l}(k) > HI \vee SOC_{n,l}(k) < LO\right)\right\}} \quad (52)$$

$$Q_{SOCmq}' = max\left\{SOC_{n,l}(k) : SOC_{n,l}(k) \in S:\left(SOC_{n,l}(k) > HI \vee SOC_{n,l}(k)\right.\right.$$
$$< LO), k \in \{1, 2, ..., T\}\right\} \quad (53)$$

Table 3
Constraint violation comparisons of CC-SMPC and DMPC methods for Case 1 offline tests.

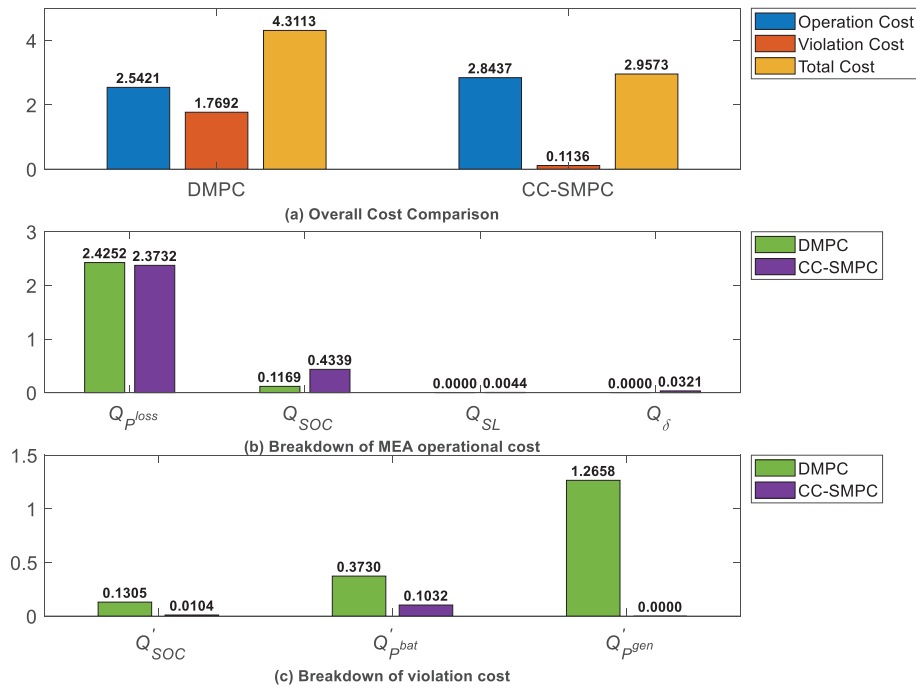| Case	ρ	Battery power constraint violation				Generator power constraint violation			
		Q_{Pbatmp}' [%]	Q_{Pbatap}' [%]	Q_{Pbatmq}' [kW]	Q_{Pbataq}' [kW]	Q_{Pgenmp}' [%]	Q_{Pgenap}' [%]	Q_{Pgenmq}' [kW]	Q_{Pgenaq}' [kW]
CC-SMPC	0.01	3	1.94	0.2318	0.0776	0	0	0	0
	0.05	8	4.69	0.2940	0.0739	5	4.41	1.3088	0.7068
	0.1	14	8.95	0.4262	0.0745	12	11.6	2.0288	0.7457
	0.2	24	17.23	0.4821	0.0921	22	20.21	2.9007	1.0991
DMPC	N.A	56	42.61	0.7743	0.1235	35	27.34	3.6729	1.2533

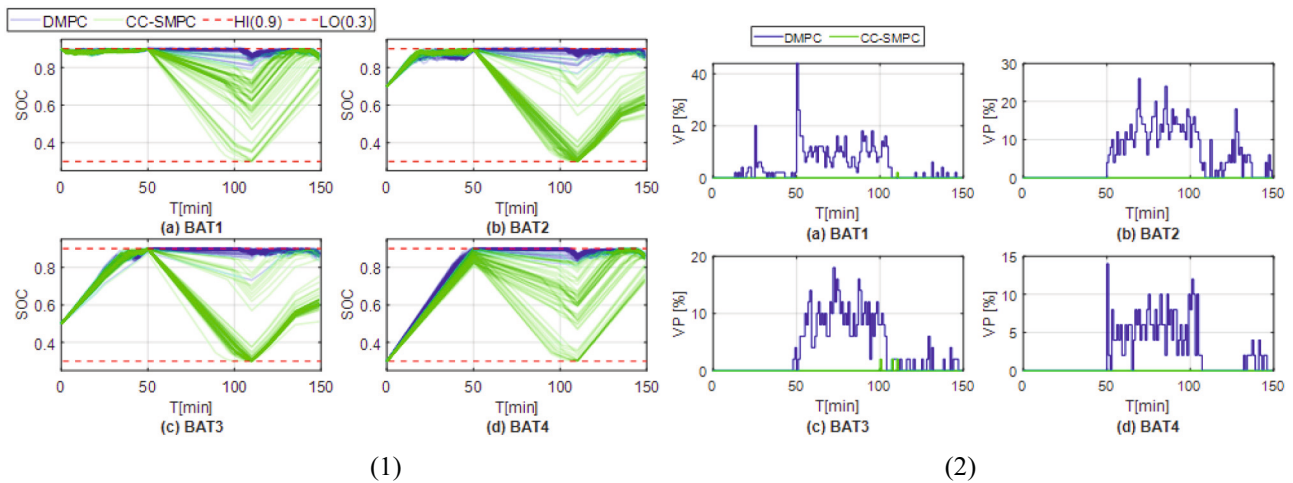**Fig. 4.** Cost comparison of online DMPC and CC-SMPC for Case 1.

Fig. 5. SOC results when adopting online DMPC and CC-SMPC for Case 1: (1) SOC changes; (2) Violation Percentage across all uncertain scenarios.

$$\begin{cases} Q'_{SOC} = v_{SOCmp}Q'_{SOCmp} + v_{SOCap}Q'_{SOCap} + v_{SOCmq}Q'_{SOCmq} + v_{SOCap}Q'_{SOCaq} \\ v_{SOCmp} + v_{SOCap} + v_{SOCmq} + v_{SOCap} = 1 \end{cases}$$

(55)

5.2. Simulation results and analysis

In the following subsections, simulation results for each case mentioned in Section 4 are evaluated and discussed.

5.2.1. Simulation results for Case 1

1) Offline scenario tests

Table 3 presents the offline simulation results for constraint violation comparisons of battery and generator power with both CC-SMPC and DMPC methods for Case 1. For the CC-SMPC approach, the test is

conducted with different violation probabilities of 1 %, 5 %, 10 %, and 20 %, with 100 uncertain load scenarios being applied for each violation probability. For the DMPC, the same uncertain load scenarios are used. According to Table 3, when ρ increases, the constraint violation indices for the battery and generator power increase by approximately the same percentage, which verifies the effectiveness of the proposed probabilistic approach for Case 1. In addition, compared to offline DMPC, all offline CC-SMPC with the selected ρ reduces the power constraint violations for batteries and generators.

2) Online scenario tests

Since generators are the only power supplies to the HV loads, to avoid generator overload situations due to the uncertain behavior of loads on the HV side, the CC-SMPC-based controller allocates less power to be transferred from the HV side to the LV side. This means that more energy from batteries will be used for supplying LV loads during peak
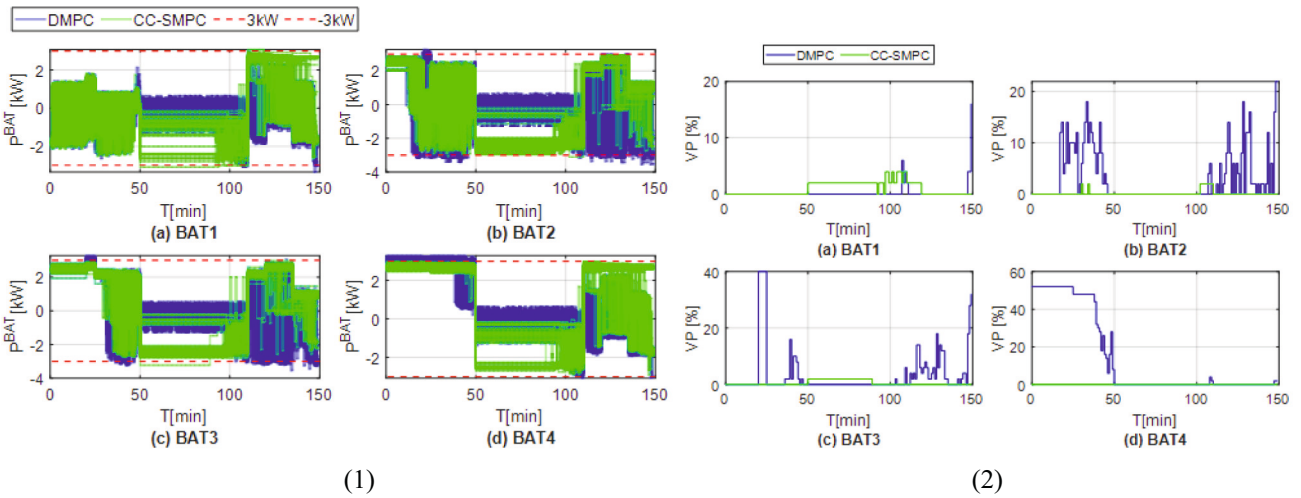
Fig. 6. Battery power results when adopting online DMPC and CC-SMPC for Case 1: (1) Battery power changes; (2) Violation Percentage among all uncertain scenarios.
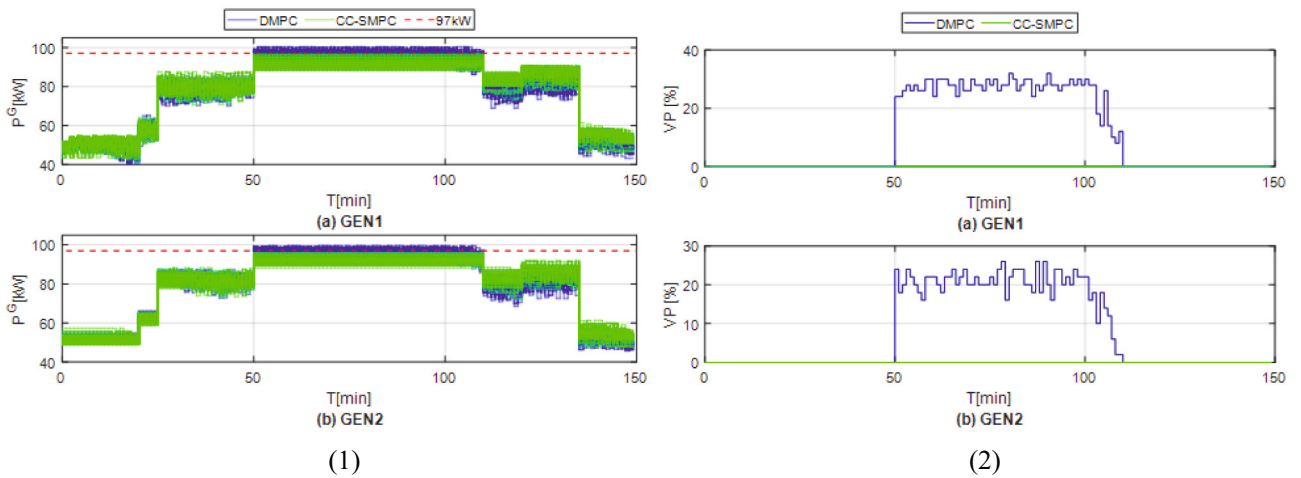

Fig. 7. Generator power results when adopting online control of DMPC and CC-SMPC for Case 1: (1) Generator power changes; (2) Violation Percentage among all uncertain scenarios.

Table 4
Failure events during the flight.

Time of fault occurrence	19 min	49 min	79 min	109 min
Failed Component	Generator 1	Cell 10	Cell 3	Battery 2

intervals. In the worst scenarios, such as low SOC conditions and high load power demand, load shedding can also be triggered. These actions lead to a higher operational cost due to low SOC levels and the

additional cost imposed by load shedding and switching activities. The performance of the DMPC and CC-SMPC methods is evaluated using 50 uncertain load scenarios. Fig. 4 demonstrates the operation cost and the violation cost for both control strategies. In general, the CC-SMPC method leads to a higher operation cost, 12 % more than the cost of the DMPC method. According to the breakdown of the operation cost represented in Fig. 4(b), the CC-SMPC strategy has an almost 3 times higher SOC cost compared to the DMPC method and a small amount of cost due to the load shedding and switching activities. However, compared to the DMPC method, the CC-SMPC reduces the total violation
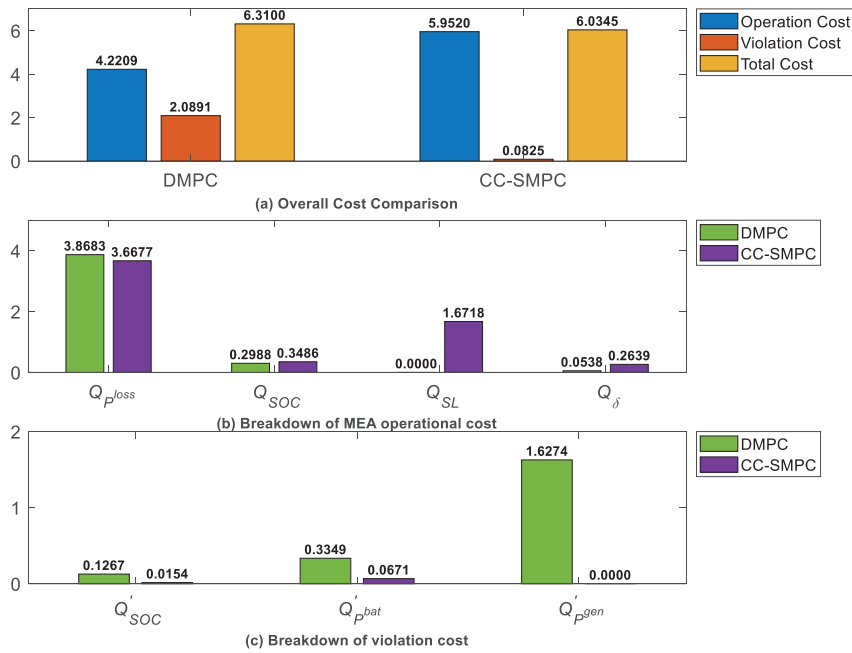
Table 5
Constraint violation comparisons of CC-SMPC and DMPC for Case 2 offline tests.

Case	ρ	Battery power constraint violation				Generator/APU power constraint violation			
		$Q_{Pbat_{mp}}{}'$ Max %	$Q_{Pbat_{ap}}{}'$ Mean %	$Q_{Pbat_{mq}}{}'$ [kW]	$Q_{Pbat_{aq}}{}'$ [kW]	$Q_{Pgen_{mp}}{}'$ Max %	$Q_{Pgen_{ap}}{}'$ Mean %	$Q_{Pgen_{mq}}{}'$ [kW]	$Q_{Pgen_{aq}}{}'$ [kW]
CC-SMPC	0.01	3	1.86	0.2283	0.0627	0	0	0	0
	0.05	8	4.92	0.2684	0.0927	5	3.52	1.2834	0.7009
	0.1	14	11.23	0.5197	0.0887	12	5.51	2.0106	0.7237
	0.2	24	15.46	0.4942	0.0889	21	7.84	2.8913	0.9843
DMPC	N.A	57	31.38	0.7473	0.1110	47	12.97	4.5762	1.4077

Fig. 8. Cost comparison of online DMPC and CC-SMPC for Case 2.

cost by 93 %, which contains a 92 % reduction in SOC violation, 72 % reduction in battery power violation, and 100 % reduction in generator power violation cost. This indicates that the DMPC method requires corrective control actions to cope with the constraint violation situations, which will lead to additional operating costs. However, this is less likely to be an optimal solution compared to the CC-SMPC method, which directly provides the solutions which explicit account for the violation probability of uncertain parameters. According to the results, CC-SMPC reduces the total cost by 31.4 % compared to the DMPC method. Fig. 5 to Fig. 7 represent the simulation results of both control techniques in all scenarios during different flight stages.

Fig. 5 presents the SOC changes over time, along with the violation percentage for both DMPC and CC-SMPC strategies when each controller is applied for 50 uncertain scenarios. Fig. 6 shows the corresponding battery power. The SOC value for batteries 1 to 4 vary from high to low levels of 0.9, 0.7, 0.5, and 0.3, respectively. As can be seen in both figures, before $t = 50$ min, when the system loads are not in their peak interval, batteries 2–4 can be charged with generator power, while battery 1 is not charged as its initial value has been set to the maximum

SOC. However, compared to the CC-SMPC method, during the charging period, the DMPC method is more likely to charge the battery with higher power values exceeding the charging power limitation (3 kW in this paper). For example, battery 4 is charged with the maximum power of around 3.3 kW by the DMPC method in 52 % of scenarios before $t = 45$ min. Likewise, for batteries 2 and 3, during $t = 20$ to $t = 25$ min, the charging power reaches 3.3 kW in 40 % and 14 % of scenarios, respectively. In addition, when the SOC becomes close to the upper bound, the battery is discharged in some time steps, to keep the SOC value within the target range. Compared to CC-SMPC, the DMPC method tends to discharge the battery with discharging power exceeding its maximum possible power limit, which indicates that the constraint violation would require corrections by adding a local controller in real situations. For example, batteries 2 and 3 have around 20 % over-discharge scenarios with a maximum power of 3.6 kW after $t = 100$ min. Compared to the battery power violation, although DMPC causes SOC violation in 10 %–40 % of scenarios from $t = 50$ min to $t = 100$ min, the violation level is low (rising to approximately 0.902) with respect to the upper bound (HI = 0.9) which is due to the MPC online feedback
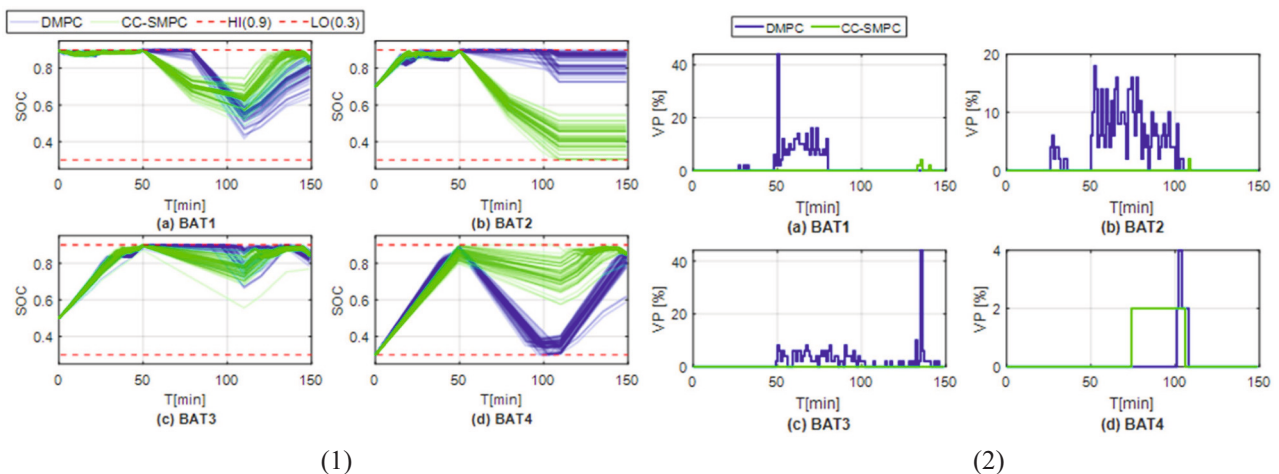

Fig. 9. SOC results when adopting online DMPC and CC-SMPC for Case 2: (1) SOC changes; (2) Violation Percentage among all uncertain scenarios.
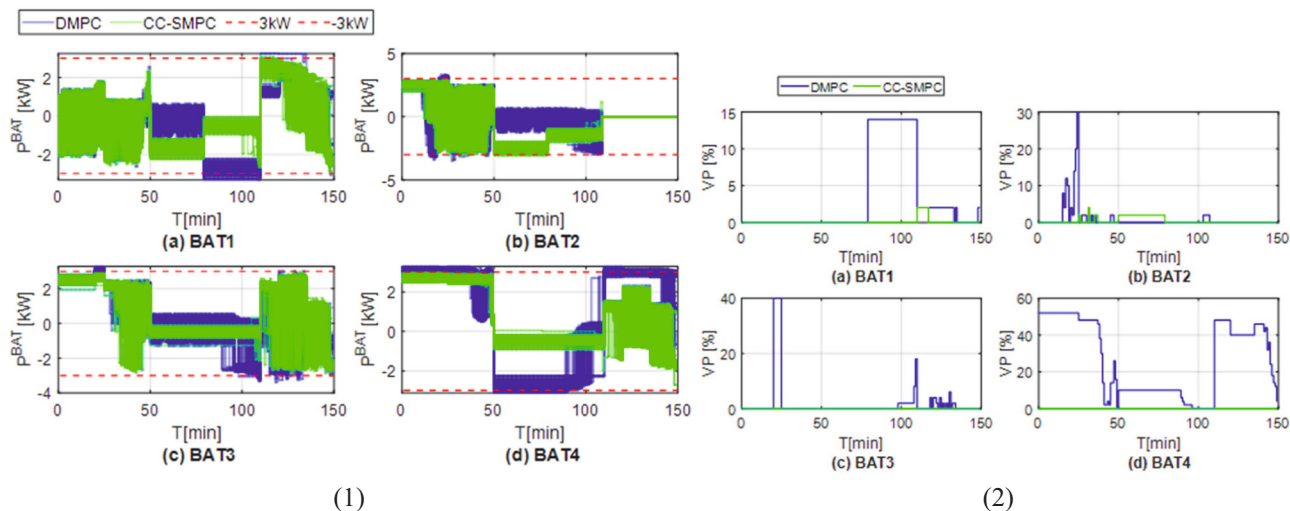
Fig. 10. Battery power results when adopting online control of DMPC and CC-SMPC for Case 2: (1) Battery power changes; (2) Violation Percentage among all uncertain scenarios.
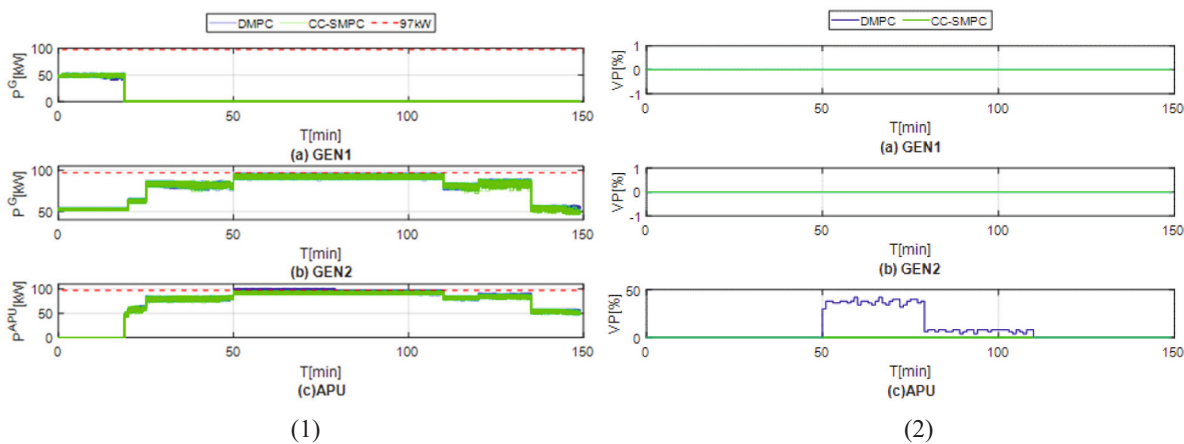

Fig. 11. Generator power results when adopting online control of DMPC and CC-SMPC for Case 2: (1) Generator power changes; (2) violation percentage among all uncertain scenarios.
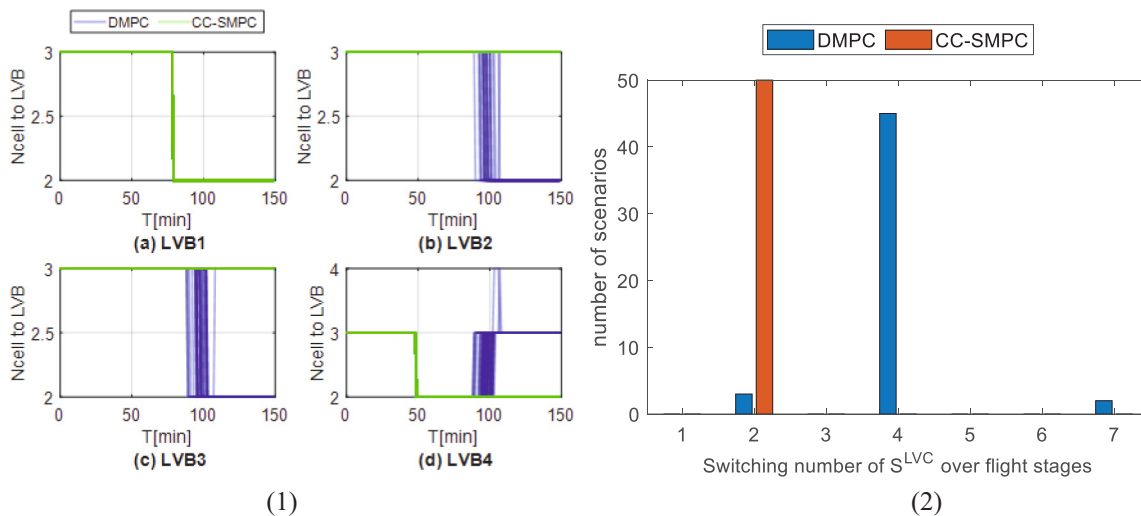

Fig. 12. Connections of cells to LV buses when adopting online DMPC and CC-SMPC for Case 2: (1) number of cells connected to each LV bus in all flight stages; (2) number of switching activities related to the connections of cells to LV bus.
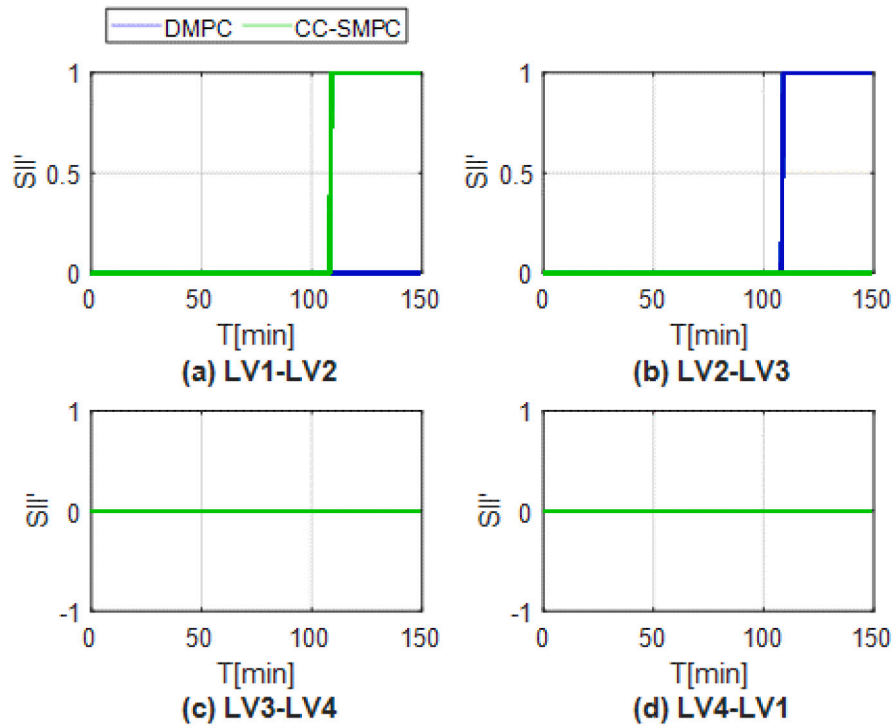
Fig. 13. Connections of LV bus interconnections with online DMPC and CC-SMPC for Case 2.
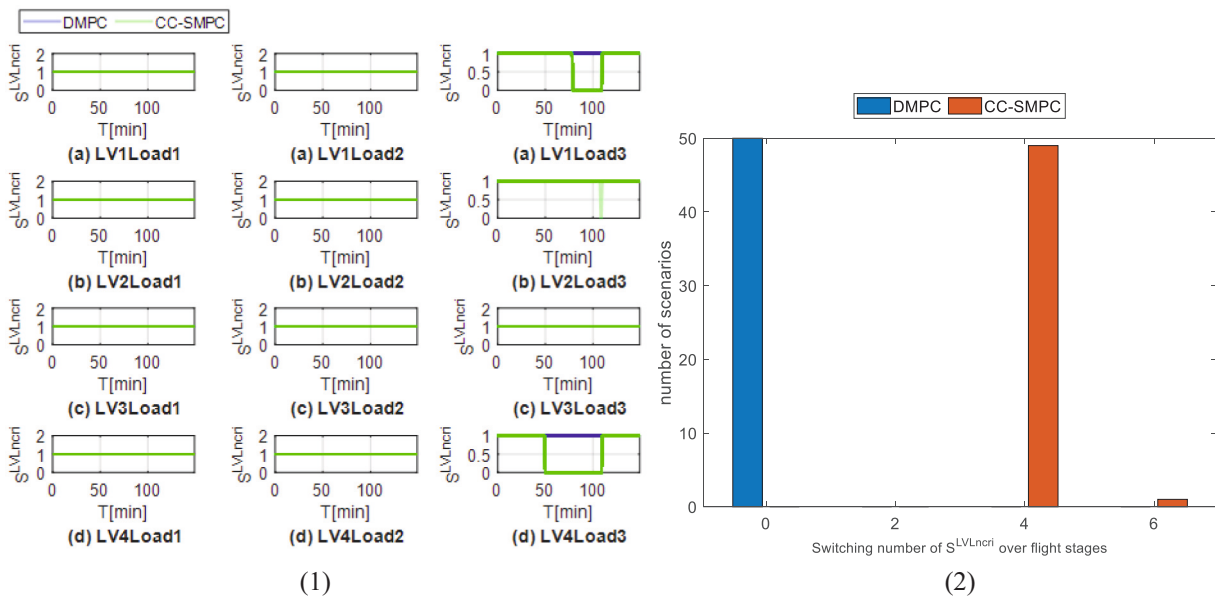

Fig. 14. Connection of LV noncritical loads when adopting online DMPC and CC-SMPC for Case 2: (1) load shedding in all flight stages; (2) number of switching activities of all LV noncritical loads.

strategy. Both DMPC and CC-SMPC online methods will correct for the SOC violation once it has occurred, however, predicting and avoiding the violation before it occurs would be far more preferable.

Fig. 7 presents both the output power of both generators and the violation percentage for the aforementioned 50 scenarios when adopting the DMPC and CC-SMPC methods. The figure shows that the power of the generators reaches its peak value from $t = 50$ to $t = 110$ min. Compared to the DMPC method, the CC-SMPC strategy controls generator operation without exceeding their maximum power limitations, discharging the batteries when necessary during this period. Although the DMPC strategy relies less on the batteries' power to avoid costs

imposed by low SOC levels, it violates the generators' power limitation in 30 % of scenarios, with a maximum power of around 100.3 kW for each generator. This indicates two potential drawbacks of the application of the DMPC method. One solution is to add another layer of control, such as a rule-based control layer, to work out how to compensate to satisfy the operation costs. This is likely to result in sub-optimal solutions. Another solution would be to design larger generators, with more power redundancy, leading to an increase in the generators' weight, which is not desirable in aircraft applications. Therefore, the CC-SMPC method can be considered to show its superiority compared to the DMPC method for Case 1 by avoiding both drawbacks.

5.2.2. Simulation results for case 2

In Case 2, in addition to considering the load uncertainty at both HV and LV sides, the following failure scenarios are also assumed during different flight stages: failure events for Generator 1, Cell 10, Cell 3, and Battery 2. In this case, in contrast to the previous cases which studied only normal system operation, the DMPC and CC-SMPC strategies are required to provide feasible solutions to cope with the components' failures. The failures listed in Table 4 are included in both offline and online testing and are assumed to occur at the specified time instances.

1) Offline scenario tests

Table 5 presents the offline simulation results for constraint violation comparison of battery and generator power with both CC-SMPC and DMPC methods for Case 2. In the failure scenarios, the APU is started in all tests with both the CC-SMPC and DMPC methods to avoid the load shedding caused by generator failure (which is further presented in the online results). The CC-SMPC and DMPC methods provide different configurations and load shedding results when cells and battery failures occur. The load shedding leads to lower load demands in the system, which leads to reducing the average constraint violation $Q_{Pbat_{ap}}'$ and $Q_{Pgen_{ap}}'$ in total for both CC-SMPC and DMPC compared to Case 1. According to Table 5, the values are consistent with the change of probability, which presents fewer violations when the probability decreases. Similar to Case 1, the DMPC method leads to higher violations compared to the CC-SMPC technique with different ρ values.

2) Online scenario tests

Fig. 8 illustrates both operating costs and constraint violation costs for the DMPC and CC-SMPC strategies evaluated by the framework introduced in Section 5.1. Each control method is applied to 50 uncertain load scenarios considering the components' failure events, while the failures occur following the aforementioned sequence. Based on the chosen evaluation weighting coefficients, the CC-SMPC approach has a 41 % higher total operation cost compared to the DMPC method, as the CC-SMPC–based solution strategy involves load shedding and switching activities for disconnection/reconnection for the loads, which is associated with higher weighting factors than the transmission switches in this study. However, compared to the DMPC method, the CC-SMPC total cost for constraint violation is reduced by 96 %, with each type of violation cost being reduced by at least 80 %. Moreover, the violation of the generator output power has been avoided 100 % of the time. In general, by adopting the CC-SMPC method the total cost has been reduced by 4.37 %. The detailed simulation results of both DMPC and SPMC strategies for all 50 testing scenarios are now presented and discussed.

Fig. 9 to Fig. 11 illustrate the SOC level of the four batteries, the batteries' power, and generators/APU power. Before the generator failure occurs (at $t = 19$ min), the system operates in normal mode, which shows the same results as Case 1. According to Fig. 11, after the failure of generator 1, the APU is started to replace the failed generator, to continue supplying the system by closing the switches at the link of the HV bus and APU bus. This has a few impacts on battery power (Fig. 10) and SOC changes (Fig. 9) before other failures occur, although the power loss slightly increases due to the bus interconnection. Before $t = 49$ min, similarly to Case 1 with the same configuration and load connection, the CC-SMPC performs better than DMPC by avoiding the battery power violation which occurs in 30 % to 50 % of scenarios in DMPC.

At t = 49 min, cell number 10 fails, which leads to the power shortage from the HV side, particularly for LV bus 4, while the system enters the high power demand interval. During this period, the DMPC and CC-SMPC strategies provide different solutions for supplying the loads at LV bus 4. The DMPC-based solution strategy tries to discharge battery number 4 with a discharging power that exceeds the maximum allowable discharging power in 10 % of scenarios, with a maximum

value of 3.2 kW. This results in decreasing the battery SOC level but avoids load shedding. On the other hand, the CC-SMPC-based solution strategy involves shedding the load with the lowest priority at the LV bus to avoid the battery power violation and keep the battery SOC at higher levels, as presented in Fig. 14. Compared to the CC-SMPC-based control in Case 1 during the same time interval, shedding the load at LV bus 4 also saves power, which is then available for charging battery 3, which is also supplied by generator 2. Since unnecessary switching activities should be avoided, the load shedding remains for 60 min and the connection status of the cells to LV buses is not changed before the occurrence of the next failure. In addition, from $t = 50$ min to $t = 79$ min, the DMPC strategy relies on the APU to supply LV buses 1 and 2, and APU maximum power violation occurs in approximately 40 % of scenarios, with the maximum violation power being 4.5 kW. On the other hand, as shown in Fig. 11- (c) the CC-SMPC method avoids 100 % of these violations.

At $t = 79$ min, cell number 3 fails, which leads to a further power shortage on the LV side, while LV bus 1, connected to this cell, is impacted directly by this failure. According to Fig. 12, after the occurrence of this failure, the number of cells connected to bus 1 is reduced from 3 to 2 in both DMPC and CC-SMPC methods. However, when adopting the DMPC strategy, the LV loads on LV bus 1 don't experience any load shedding, instead the connected battery is over-discharged in 14 % of scenarios with the maximum power of 3.3 kW, and the APU is overloaded in 8 % of scenarios with the maximum power of 98.3 kW. The CC-SMPC strategy sheds the lowest priority load at this LV bus, which avoids all of the power excess situations and keeps the SOC level 10 % higher than the SOC in the DMPC method. This is presented in Fig. 14 (1-a). In addition, comparing the SOC changes for this period in Fig. 9, with the DMPC method, battery 4 has been discharged close to the lower bound during all cruising stages, and additional transmission switching activities are conducted to avoid the SOC dropping below the lower bound. In contrast, the CC-SMPC method avoids these switching activities because the lowest priority load for battery 4 remains shed. In summary, by predicting that the maximum power may be exceeded, a situation which is important to avoid if possible, the CC-SMPC method sheds the lowest priority load to avoid this happening. This also results in greater SOC available later in the flight.

At $t = 109$ min, when Battery 2 fails, both DMPC and CC-SMPC methods disconnect this battery and stop charging/discharging it. When adopting the DMPC method, LV bus 2 and LV bus 3 are connected to supply the load at LV bus 2, while the CC-SMPC method connects LV bus 2 with LV bus 1, as presented in Fig. 13. This difference is mainly caused by the average SOC level, which is accumulated differently in previous steps. At this stage, all loads which were shed by the CC-SMPC method are re-connected to the system, which causes additional switching activities. Fig. 14 (2) shows that among 50 scenarios, the CC-SMPC control leads to 48 scenarios with 4 LV loads switching activities, and 2 scenarios with 6 LV loads switching activities. However, the DMPC method again leads to a battery power limit violation in 48 % of scenarios, as well as the violation of the SOC upper bound in 44 % of scenarios, which is reduced to 2 % with the CC-SMPC method.

As a conclusion for Case 2, the proposed CC-SMPC method is capable of coping with multiple failure scenarios. Compared to the DMPC method, when power shortages happen in the system because of failures, the CC-SMPC method results in more conservative operating strategies, such as more load shedding but less SOC reduction compared to the DMPC method. In addition, similarly to Case 1, the CC-SMPC method performs better in controlling the system with fewer constraint violations.

6. Conclusions

This paper studied the optimal operational control of an EPS integrated with modular converters and multiple ESSs on an MEA in both normal and faulty situations, targeting the improvement of the

performance of the system in terms of power losses, energy storage, and load shedding as well as reducing the number of switching activities. For dealing with the uncertainty of load power demand on both HV and LV buses, the operational management problem is formulated in the framework of CC-SMPC. Two sources of uncertainty are studied, including the uncertainty of load power demand on both LVBs and HVBs. Based on the uncertainty propagation in normal/faulty conditions, different probabilistic constraints are proposed for each case. Moreover, a comprehensive Monte-Carlo-based offline and online simulation study is conducted for both DMPC and CC-SMPC methods, and the results are evaluated with the proposed multi-dimension evaluation framework. Based on the comparison of the operational costs and the violation costs in normal and faulty cases, the proposed CC-SMPC improves the violation costs and the overall costs compared to the DMPC technique in both cases.

CRediT authorship contribution statement

Xin Wang: Conceptualization, Methodology, Software, Formal analysis, Visualization, Investigation, Validation, Writing – original draft, Writing – review & editing. **Najmeh Bazmohammadi:** Methodology, Software, Formal analysis, Data curation, Investigation, Writing – review & editing. **Jason Atkin:** Resources, Methodology, Writing – review & editing, Supervision. **Serhiy Bozhko:** Resources, Supervision, Project administration, Funding acquisition, Writing – review & editing. **Josep M. Guerrero:** Supervision, Project administration, Writing – review & editing.

Declaration of competing interest

The authors declare that they have no known competing financial interests or personal relationships that could have appeared to influence the work reported in this paper.

Data availability

Data will be made available on request.

Appendix A

Table 6
Mean value load profile based on flight stages with indices in Fig. 3.

Load types [kW]	Load indices	Ground (20 min)	Take off (5 min)	Climb (25 min)	Cruise (60 min)	Descent (10 min)	Loiter (15 min)	Landing (15 min)
HV Critical Loads	HVL1[1], HVL2[1]	10.01	29.58	22.20	21.40	22.20	27.21	30.00
LV Critical Loads	LVL1[1], LVL4[1]	1.78	1.94	2.07	3.00	2.07	2.07	1.94
	LVL2[1], LVL3[1]	3.00	2.50	2.50	2.50	2.50	2.50	3.00
HV HP Loads	HVL1[2], HVL2[2]	4.89	8.34	24.00	24.00	24.00	24.00	0.87
LV HP Loads	LVL1[2], LVL4[2]	1.40	1.30	1.30	1.30	1.60	0.80	0.80
	LVL2[2], LVL3[2]	0.50	0.50	0.50	0.50	1.50	1.00	2.20
HV MP Loads	HVL1[3], HVL2[3]	15.00	3.42	14.16	14.60	14.16	14.16	3.42
LV MP Loads	LVL1[3], LVL4[3]	0.50	0.35	0.35	2.00	0.35	0.35	0.35
	LVL2[3], LVL3[3]	0.70	0.70	1.50	2.50	0.50	0.50	0.50
HV LP Loads	HVL1[4], HVL2[4]	6.00	6.00	6.00	18.00	6.00	6.00	6.00
LV LP Loads	LVL1[4], LVL4[4]	1.00	0.70	1.50	2.20	0.50	0.50	1.50
	LVL2[4], LVL3[4]	2.00	1.50	2.00	3.00	2.00	2.00	2.00

References

[1] FAA, Office of Environment and Energy January 2015, 2015.
[2] Airbus, Environment matters for the future of aerospace, Airbus Environ. (2019) 1–26.
[3] X. Wang, J. Atkin, C. Hill, S. Bozhko, Power allocation and generator sizing optimisation of more-electric aircraft on-board electrical power during different flight stages, AIAA Propuls. Energy Forum Expo. 2019 (August) (2019) 1–10.
[4] V. Madonna, P. Giangrande, M. Galea, Electrical power generation in aircraft: review, challenges and opportunities, IEEE Trans. Transp. Electrif. 7782 (665468) (2018), 1-1.
[5] S. Bozhko, M. Liserre, K. Al-Haddad, G. Buticchi, P. Wheeler, On-board microgrids for the more electric aircraft - technology review, IEEE Trans. Ind. Electron. 66 (7) (2018), 1-1.
[6] P. Wheeler, S. Bozhko, The more electric aircraft, IEEE Electrif. Mag. (December) (2014) 1–7.
[7] C. Spagnolo, S. Sumsurooah, S. Bozkho, Advanced smart grid power distribution system for more electric aircraft application, in: Proc. - ICOECS 2019 2019 Int. Conf. Electrotech. Complexes Syst, 2019.
[8] S. Sumsurooah, ENIGMA-A centralised supervisory controller for enhanced onboard electrical energy management with model in the loop demonstration, Energies 14 (17) (2021).
[9] A. Alsharif, C.W. Tan, R. Ayop, K.Y. Lau, A.M.D. Dobi, A rule-based power management strategy for Vehicle-to-Grid system using antlion sizing optimization, J. Energy Storage 41 (June) (2021) 102913.
[10] H. Mohammadi, M. Mohammadi, A. Ghasemi, Optimal configuration planning of rule and optimization-based driven storage coupled micro cogeneration systems by the implementation of constraint programming, J. Energy Storage 48 (October) (2022) 103934, 2021.
[11] C. Wang, R. Liu, A. Tang, Energy management strategy of hybrid energy storage system for electric vehicles based on genetic algorithm optimization and temperature effect, J. Energy Storage 51 (March) (2022), 104314.
[12] M.R. Basir Khan, R. Jidin, J. Pasupuleti, Multi-agent based distributed control architecture for microgrid energy management and optimization, Energy Convers. Manag. 112 (2016) 288–307.
[13] Y. Zhang, Y. Yu, R. Su, J. Chen, Power scheduling in more electric aircraft based on an optimal adaptive control strategy, IEEE Trans. Ind. Electron. (December 2019) (2019), 1-1.
[14] T. Assaf, A.H. Osman, M.S. Hassan, H. Mir, Fair and efficient energy consumption scheduling algorithm using tabu search for future smart grids, IET Gener. Transm. Distrib. 12 (3) (2018) 643–649.
[15] X. Lü, et al., Energy management of hybrid electric vehicles: a review of energy optimization of fuel cell hybrid power system based on genetic algorithm, Energy Convers. Manag. 205 (January) (2020), 112474.
[16] J. Zhu, X. Cui, W. Ni, Model predictive control based control strategy for battery energy storage system integrated power plant meeting deep load peak shaving demand, J. Energy Storage 46 (August) (2022) 103811, 2021.
[17] M. Maasoumy, P. Nuzzo, F. Iandola, M. Kamgarpour, A. Sangiovanni-Vincentelli, C.J. Tomlin, Optimal load management system for Aircraft Electric Power distribution, IEEE Conf. Decis. Control (2013) 2939–2945.
[18] Z. Jiang, S.A. Raziei, Hierarchical model predictive control for real-time energy-optimized operation of aerospace systems, AIAA Propuls. Energy Forum Expo. 2019 (August) (2019) 1–16.

[19] W. Dunham, B. Hencey, A.R. Girard, I. Kolmanovsky, Distributed model predictive control for more electric aircraft subsystems operating at multiple time scales, IEEE Trans. Control Syst. Technol. 28 (6) (2020) 2177–2190.

[20] B. Otomega, A. Marinakis, M. Glavic, T. Van Cutsem, Model predictive control to alleviate thermal overloads, IEEE Trans. Power Syst. 22 (3) (2007) 1384–1385.

[21] F. Borrelli, A. Bemporad, M. Morari, Predictive Control for Linear and Hybrid Systems, Cambridge University Press, 2017.

[22] B. Shahsavari, M. Maasoumy, A. Sangiovanni-Vincentelli, R. Horowitz, Stochastic model predictive control design for load management system of aircraft electrical power distribution, in: 2015 Am. Control Conf, 2015, pp. 3649–3655.

[23] P. Kou, D. Liang, L. Gao, Distributed EMPC of multiple microgrids for coordinated stochastic energy management, Appl. Energy 185 (2017) 939–952.

[24] R.R. Appino, J.Á.González Ordiano, R. Mikut, T. Faulwasser, V. Hagenmeyer, On the use of probabilistic forecasts in scheduling of renewable energy sources coupled to storages, Appl. Energy 210 (October 2017) (2018) 1207–1218.

[25] X. Wang, Y. Liu, L. Xu, J. Liu, H. Sun, A chance-constrained stochastic model predictive control for building integrated with renewable resources, Electr. Power Syst. Res. 184 (February) (2020) 106348.

[26] F. Oldewurtel, L. Roald, G. Andersson, C. Tomlin, Adaptively constrained stochastic model predictive control applied to security constrained optimal power flow, Proc. Am. Control Conf. 2015-July (c) (2015) 931–936.

[27] N. Bazmohammadi, A. Tahsiri, A. Anvari-Moghaddam, J.M. Guerrero, Stochastic predictive control of multi-microgrid systems, IEEE Trans. Ind. Appl. 55 (5) (2019) 5311–5319.

[28] J. Li, L. Lin, Y. Xu, S. Zhou, D. Zhu, J. Liang, Probability efficient point method to solve joint chance-constrained unit commitment for multi-area power systems with renewable energy, IEEE Trans. Power Syst. 8950 (51977042) (2022), 1-1.

[29] Y.Y. Hong, G.F.D. Apolinario, T.K. Lu, C.C. Chu, Chance-constrained unit commitment with energy storage systems in electric power systems, Energy Rep. 8 (2022) 1067–1090.

[30] P.K. Mianaei, M. Aliahmadi, S. Faghri, M. Ensaf, A. Ghasemi, A.A. Abdoos, Chance-constrained programming for optimal scheduling of combined cooling, heating, and power-based microgrid coupled with flexible technologies, Sustain. Cities Soc. 77 (July) (2022) 103502, 2021.

[31] G. Wu, Chance-constrained energy-reserve co-optimization scheduling of wind-photovoltaic-hydrogen integrated energy systems, Int. J. Hydrogen Energy (2022).

[32] S. Esmaeili, A. Anvari-Moghaddam, S. Jadid, J.M. Guerrero, A stochastic model predictive control approach for joint operational scheduling and hourly reconfiguration of distribution systems, Energies 11 (7) (2018).

[33] Y. Zhang, J. Wang, B. Zeng, Z. Hu, Chance-constrained two-stage unit commitment under uncertain load and wind power output using bilinear benders decomposition, IEEE Trans. Power Syst. 32 (5) (2017) 3637–3647.

[34] D. van der Meer, G.C. Wang, J. Munkhammar, An alternative optimal strategy for stochastic model predictive control of a residential battery energy management system with solar photovoltaic, Appl. Energy 283 (October) (2021) 116289, 2020.

[35] Y. Zhang, F. Meng, R. Wang, W. Zhu, X.J. Zeng, A stochastic MPC based approach to integrated energy management in microgrids, Sustain. Cities Soc. 41 (May) (2018) 349–362.

[36] N. Bazmohammadi, A. Anvari-Moghaddam, A. Tahsiri, A. Madary, J.C. Vasquez, J. M. Guerrero, Stochastic predictive energy management of multi-microgrid systems, Appl. Sci. 10 (14) (2020).

[37] M. Nasir, A. Rezaee Jordehi, S.A.A. Matin, V.S. Tabar, M. Tostado-Véliz, S. A. Mansouri, Optimal operation of energy hubs including parking lots for hydrogen vehicles and responsive demands, J. Energy Storage 50 (March) (2022), 104630.

[38] S.A. Mansouri, A multi-stage joint planning and operation model for energy hubs considering integrated demand response programs, Int. J. Electr. Power Energy Syst. 140 (March) (2022).

[39] S.A. Mansouri, A. Ahmarinejad, E. Nematbakhsh, M.S. Javadi, A.Esmaeel Nezhad, J.P.S. Catalão, A sustainable framework for multi-microgrids energy management in automated distribution network by considering smart homes and high penetration of renewable energy resources, Energy 245 (2022).

[40] A. Rezaee Jordehi, V.S. Tabar, S.A. Mansouri, M. Nasir, S. Pirouzi, A risk-averse two-stage stochastic model for planning retailers including self-generation and storage system, J. Energy Storage 51 (March) (2022), 104380.

[41] W. Dunham, B. Hencey, I. Kolmanovsky, A. Girard, Scenario based stochastic MPC for more electric aircraft coordinated engine and power management, Proc. Am. Control Conf. 2019-July (2019) 4223–4228.

[42] Y. Zhang, J. Chen, Y. Yu, Distributed power management with adaptive scheduling horizons for more electric aircraft, Int. J. Electr. Power Energy Syst. 126 (PA) (2021), 106581.

[43] A. Carolina Luna, et al., Online energy management systems for microgrids: experimental validation and assessment framework, IEEE Trans. Power Electron. 8993 (c) (2017) 1–15.

[44] M. Elkazaz, M. Sumner, E. Naghiyev, S. Pholboon, R. Davies, D. Thomas, A hierarchical two-stage energy management for a home microgrid using model predictive and real-time controllers, Appl. Energy 269 (April) (2020), 115118.

[45] M.S. Mahmoud, Chapter 1 - introduction, in: M.S.B.T.-A.C.D. with A. to E. S. Mahmoud (Ed.), Advanced Control Design with Application to Electromechanical Systems, Butterworth-Heinemann, 2018, pp. 1–41.

[46] M. Issa, M. Rezkallah, A. Ilinca, H. Ibrahim, 4 - Grid integrated non-renewable based hybrid systems: control strategies, optimization, and modeling, in: M. Lo Faro, O. Barbera, G.B.T.-H.T. for P.G. Giacoppo (Eds.), Hybrid Energy Systems, Academic Press, 2022, pp. 101–135.

[47] M. Maasoumy, P. Nuzzo, F. Iandola, M. Kamgarpour, A. Sangiovanni-Vincentelli, C.J. Tomlin, Optimal load management system for aircraft electric power distribution, in: IEEE Conference on Decision and Control, 2013, pp. 2939–2945.

[48] X. Wang, J. Atkin, S. Bozhko, C. Hill, Application of a MILP-based algorithm for power flow optimisation within more-electric aircraft electrical power systems, in: 2019 21st Eur. Conf. Power Electron. Appl. EPE 2019 ECCE Eur, 2019 p. P.1-P.8.

[49] A.R. Jordehi, How to deal with uncertainties in electric power systems? A review, Renew. Sustain. Energy Rev. 96 (June 2017) (2018) 145–155.

[50] J. Kirchner, Data Analysis Toolkit #5: Uncertainty Analysis and Error Propagation, 2016.

[51] L. Blackmore, H. Li, B. Williams, A probabilistic approach to optimal robust path planning with obstacles, Proc. Am. Control Conf. 2006 (2006) 2831–2837.